

SBAMDT: Bayesian Additive Decision Trees with Adaptive Soft Semi-multivariate Split Rules

Stamatina Lamprinakou¹, Huiyan Sang¹, Bledar A. Konomi², and Ligang Lu³

¹Department of Statistics, Texas A&M University, College Station, USA ,
matina@tamu.edu, huiyan@stat.tamu.edu

²Department of Mathematical Sciences, University of Cincinnati, Cincinnati, OH,
USA , konomibr@ucmail.uc.edu

³Shell International Exploration and Production Inc, Houston, TX, USA ,
ligang.lu@shell.com

January 20, 2025

Abstract

Bayesian Additive Regression Trees [BART, Chipman et al., 2010] have gained significant popularity due to their remarkable predictive performance and ability to quantify uncertainty. However, standard decision tree models rely on recursive data splits at each decision node, using deterministic decision rules based on a single univariate feature. This approach limits their ability to effectively capture complex decision boundaries, particularly in scenarios involving multiple features, such as spatial domains, or when transitions are either sharp or smoothly varying. In this paper, we introduce a novel probabilistic additive decision tree model that employs a soft split rule. This method enables highly flexible splits that leverage both univariate and multivariate features, while also respecting the geometric properties of the feature domain. Notably, the probabilistic split rule adapts dynamically across decision nodes, allowing the model to account for varying levels of smoothness in the regression function. We demonstrate the utility of the proposed model through comparisons with existing tree-based models on synthetic datasets and a New York City education dataset.

Keywords: Bayesian additive regression trees, Complex Domains, Graph Partitions, Minimum Spanning Tree, Soft Clustering, Spatial Nonparametric Regression.

1 Introduction

We consider a non-parametric regression problem with response $Y \in R$ and a number of features with known multivariate structures, $s \in \mathcal{M}$ (structured) and unknown structures, $\mathbf{x} \in \mathcal{X} \subseteq R^p$, $p > 0$ (unstructured) ,

$$Y = f(\mathbf{d}) + \epsilon, \quad \mathbf{d} = (\mathbf{s}, \mathbf{x}), \quad \epsilon \stackrel{\text{iid}}{\sim} N(0, \sigma^2), \quad (1)$$

where $f : \mathcal{D} \rightarrow R$ is an unknown function defined on the joint input feature space $\mathcal{D} \subseteq \mathcal{M} \times \mathcal{X}$, and σ^2 is an unknown noise variance. For example, in a spatial nonparametric regression problem where the response variable Y is the housing price, the structured multivariate features \mathbf{s} represent the spatial coordinates, and the unstructured features \mathbf{x} consist of other house features. Here, we allow the domain of the structured features to have complex geometries, such as road networks, brain cortical surfaces, and cities with inner lakes. The goal is to predict the response value at new locations as well as understand the relationships between features and response. Such problems find wide applications in real estate, public health, social sciences, and environmental studies, to name a few.

Various frequentist and Bayesian methods that employ an ensemble of trees have become popular approaches for estimating nonparametric function $f(\cdot)$. Boosting [Freund and Schapire, 1997], bagging [Breiman, 1996], and random forests [Breiman, 2001] are examples of frequentist techniques. The Bayesian Additive Regression Trees (BART) model [Chipman et al., 2010] has also gained widespread attention because of its exceptional performance and the resulting uncertainty measures. The BART model has been applied and extended to various contexts including nonparametric normal response mean regression [Chipman et al., 2010], classification [Chipman et al., 2010, Zhang and Härdle, 2010, Kindo et al., 2016], variable selection [Chipman et al., 2010, Bleich et al., 2014, Linero, 2018], estimation of monotone functions [Chipman et al., 2021], causal inference [Hill, 2011], survival analysis [Sparapani et al., 2016], heteroscedasticity [Bleich and Kapelner, 2014, Pratola et al., 2016], analysis of log-linear models [Murray, 2021] and estimating the intensity of a Poisson process [Lamprinakou et al., 2023]. Several theoretical studies of BART models [Ročková and van der Pas, 2020, Ročková and Saha, 2019, Linero and Yang, 2018] have recently established the posterior convergence rates to provide asymptotic justifications of these methods.

However, the axis-alignment characteristic of the BART model is a major limitation for the scenarios we considered in (1): the imposed prior on the trees only allows to split the feature space using one feature at a time, which can only partition the domain into hyper-rectangular regions, restricting the model’s flexibility to account for dependence structures of multivariate features in complex domains when making splits. Numerous frequentist papers have emerged proposing methods for dealing with the axis-alignment effects of decision trees [Ge et al., 2019, Fan et al., 2016, Tomita et al., 2020, Rainforth and Wood, 2015, Rodriguez et al., 2006, Blaser and Fryzlewicz, 2021, 2016]. Bayesian non-parametric methods have also been developed to allow more flexible non-axis-aligned partitioning, including the Ostomachion process [Fan et al., 2016], the Random Tessellation Process [Ge et al., 2019] and the Bayesian Additive Voronoi Tessellations [Stone and Gosling, 2024]. To address this limitation in the BART framework, Maia et al. [2024] incorporate Gaussian process priors for the predictions at each terminal node of the trees.

Luo et al. [2022] introduced the Bayesian additive semi-multivariate decision trees (BAMDT) model to overcome the BART model’s axis-alignment limitation. A semi-multivariate decision tree (sMDT) introduced by Luo et al. [2022] divides the joint input feature space \mathcal{D} into disjoint subsets using multivariate splits for structured features and univariate splits for unstructured features. The multivariate splits provide pliable-shaped partitions that respect the intrinsic geometry and the boundary conditions. However, BAMDT cannot adapt to higher smoothness levels of the unknown regression function of interest, which hinders its performance in many application problems where spatial patterns in some areas are rather smooth. Recently, Linero [2018] proposed an extension of the original axis-parallel BART model, called the soft BART (SBART) model, which introduced

a soft split scheme to replace the hard axis-parallel split rule to allow the model to capture a higher degree of smoothness in the unknown regression function. They proved that the posterior distribution of the nonparametric function f concentrates around any unknown true function in the α -Hölder space, for any $\alpha > 0$, at near minimax rate.

Motivated by the success of SBART, we develop a new Bayesian additive decision tree model, called SBAMDT, for modeling nonparametric functions in (1) with both structured and unstructured features. We introduce a novelty decision rule that assumes a mixture of hard and soft decisions at each internal node while allowing the adaptive soft split decision to depend on multivariate features. The model is capable of generating a decision boundary at each decision node that either has sharp changes or adaptive smooth transitions. We highlight that our soft decision rule has two major differences from SBART. First, SBART enforces a soft decision rule on every node, while SBAMDT learns a node-specific decision in each tree that permits some internal nodes to make hard decisions. Second, the soft data assignment probability in SBART depends on the distance from a univariate feature value to the cut point. However, such distance is not easily generalized to the multivariate feature manifold case. SBAMDT takes into account both structured and unstructured features, where To address this challenge, we propose a new approach using distances from each observation to their neighboring reference knot sets to find the probabilities of going left and right at each internal node.

The outline of the paper is as follows. Section 2 is a review of sMDT used in Luo et al. [2022]. Section 3 introduces the adaptive soft Semi-Multivariate Decision Tree, and Section 4 presents the proposed inference algorithm. Sections 5 and 6 present the application of the algorithm to synthetic data and real data sets, respectively. Section 7 provides our conclusions.

2 Review of Semi-Multivariate Decision Tree

We start by reviewing the notion of a binary tree in order to present the definition of the soft semi-multivariate decision tree. A binary decision tree is a type of tree-data structure that is made up of terminal nodes (also called leaves) and internal nodes. Each internal node η is associated with a subset of data, denoted as D_η , and a decision rule that splits η into two offspring nodes η_1 and η_2 . Accordingly, the feature space is split recursively into disjoint subsets, each of which is associated with a terminal node, following the decision path from the root to the leaf.

Conventionally, the decision rule at an internal tree node has the form $x > c$ or $x < c$ using only one feature x at a time, where c is the cut point in the domain of x . Luo et al. [2022] introduced the semi-multivariate decision tree (sMDT) that allows an internal node to split either based on multivariate structured features, $\mathbf{s} \in \mathcal{M}$ or a univariate unstructured feature, $x \in \mathcal{X} \subseteq R^p$. Luo et al. [2022] modeled the univariate split following the same method as in standard BART introduced by Chipman et al. [2010]. In a multivariate split, Luo et al. [2022] employs a bipartition model via predictive spanning trees. Specifically, a random spanning tree graph is constructed connecting a set of reference points from the multivariate structured feature space. A graph bipartition model is then developed to split the finite set of reference points. For any arbitrary given data, it is assigned to its nearest reference point in the space of \mathcal{M} . Accordingly, the input feature space is recursively partitioned into subspaces with much more flexible shapes than hyper-rectangulars by standard BART. Luo et al. [2022] illustrated the great utility of this method for spatial regression problems on various domains.

However, there are two main drawbacks of the method proposed in Luo et al. [2022]. First, due to the hard assignment nature of the decision rule, sMDT cannot adapt to the higher smoothness levels of the unknown regression function of interest. Indeed, previous work has shown that the use of piecewise constant basis functions in traditional BART models enables only adaptation to functions in Hölder space which at most have smoothness $\alpha < 1$. However, many applications problems involving spatial data may have smoother spatial variations in certain local areas. Second, Luo et al. [2022] employed the minimum spanning tree (MST) of the k nearest neighbour graph (k -NN) which requires the computation of the geodesic distance between points. Although the geodesic distance has the advantage of respecting manifold structures, it is usually more difficult to compute than the Euclidean distance, which hinders the scalability of sMDT for large-scale data sets.

3 Adaptive Soft Semi-Multivariate Additive Decision Trees

We propose a new adaptive sMDT with a mixture of hard and soft decision types to address the two limitations of the original sMDT. The latent regression function $f(\cdot)$ in (1) is modeled by a sum of m hard-soft Semi-Multivariate Decision Trees,

$$f(\mathbf{d}) = \sum_{h=1}^m g(\mathbf{d}; T^{(h)}, \mathbf{M}^{(h)}),$$

where $g(\mathbf{d}; T^{(h)}, \mathbf{M}^{(h)})$ denotes the h -th hard-soft sMDT weak learner, $T^{(h)}$ denotes the topology of the decision tree, $\mathbf{M}^{(h)} = (\mu_{h1}, \dots, \mu_{hL_h})$ is a collection of leaf parameters and L_h is the number of leaves.

We begin by introducing the hard partition model for splitting a finite set of reference knots on \mathcal{D} , which shall be used in Section 3.2 to define the mixture of hard and soft split rules to partition the domain \mathcal{D} and build the probabilistic assignment of observations based on a new distance metric.

3.1 Hard semi-multivariate decision rule model of reference points

Let $D^* = \{(x_1^*, s_1^*), \dots, (x_t^*, s_t^*)\} \subseteq \mathcal{D}$ be a finite set of reference knots on \mathcal{D} . In this study, we draw D^* by randomly sampling a subset of the observed features. We propose a generative prior to recursively split D^* , starting with a root node including the entire D^* . A leaf node is selected for further splitting with probability $p_{\text{split}}(\eta)$. If a node is chosen to split, a *multivariate* split using the structured features \mathbf{s}^* is performed with probability p_m ; otherwise, a *univariate* split using x^* is performed.

In a univariate split, D_η^* is divided into

$$D_{\eta,1}^* = \{(x^*, \mathbf{s}^*) \in D_\eta^* : x_{j(\eta)}^* \leq c_\eta\}, \quad D_{\eta,2}^* = D_\eta^* \setminus D_{\eta,1}^*$$

where $x_{j(\eta)}^*$ is the j th structured feature and c_η the split value of the rule at node η . For each unstructured feature, we utilize 100 grid points that are equally spaced as potential univariate split cutoff values. After uniformly choosing one of the unstructured features, a uniform selection is made from the available split values associated with that feature.

In a multivariate split, we assume there is a spanning tree graph, G_T^* , whose vertex corresponds to each reference point and edge set encodes the neighborhood structure of the reference points in the manifold multivariate structured feature space \mathcal{M} . Spanning tree enjoys many nice properties for the partition problems of structured data [Luo et al., 2022]. Removing one edge from a spanning tree, we easily obtain a contiguous bipartition of G_T^* into two sub-spanning trees whose vertex sets are connected components, which is ideal for obtaining recursive bipartitions of reference points needed in decision tree models. Figure 1(a) shows an example of the semi-multivariate decision tree split that includes both multivariate and univariate splits. Figure 1(b) show an example of a bipartition of G_T^* that connects spatial bins covering Texas, USA, and the resulting two disjoint reference point sets after removing an edge.

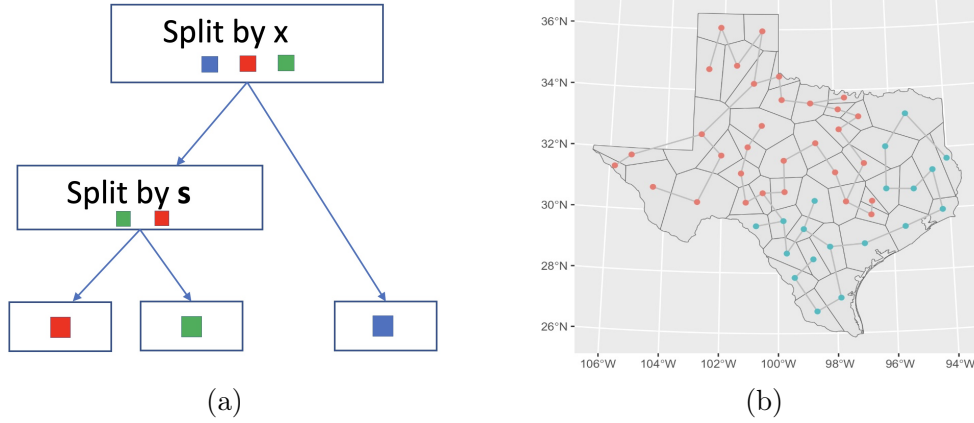


Figure 1: (a) An example of a semi-multivariate decision tree; (b) A bipartition of the spanning tree graph G_T^* into two disjoint reference point sets represented by red and blue colors, respectively.

An important component of the method is the use of the spanning tree. First, we construct a weighted adjacency graph among reference points and then generate its minimum spanning tree, which is defined as the spanning tree minimizing the total edge weight. To address the shortcomings of using geodesic distance-based k-NN graphs as the adjacency graph, we consider the idea of manifold embedding via a graph Laplacian, allowing one to use the ordinary Euclidean distance in the embedded space to approximate distances on the original manifold and construct [Crane et al., 2020]. Specifically, we first construct the initial similarity graph by connecting all points on $S^* = \{s_1^*, \dots, s_t^*\}$ with each other and weighting all edges by their similarity, given by the Gaussian function $f_s(s_i^*, s_j^*) = e^{-\|s_i^* - s_j^*\|^2}$. We then compute the normalized graph Laplacian L [Shi and Malik, 2000]. Let U be the matrix containing the k eigenvectors of L corresponding to the k smallest non-zero eigen-values, and $\tilde{S}^* = \{u_1^*, \dots, u_t^*\}$ be the resulting embedded coordinates of the structured reference knots set S^* , where u_i^* corresponds to the i -th row of the matrix U . Embedding via Laplacian graphs has been used in relation to dimensionality reduction, data representation, and diffusion processes [Coifman and Lafon, 2006, Belkin and Niyogi, 2003, Göbel and Jagers, 1974]. Dunson et al. [2022] recently defined the notion of graph-based Gaussian processes, where the covariance matrix is constructed by such an embedding.

At each node η , let S_η^* and \tilde{S}_η^* denote the structured reference knots subset on manifold and the embedded structured reference knots subset associated with η , respectively. The generative bipartition prior for the multivariate split proceeds as follows: we randomly pick two distinct

structured reference knots in \tilde{S}_η^* , denoted as u^* and t^* . There exists a unique path in G_T^* connecting these two knots. By randomly removing an edge from this path, we obtain two disjoint subsets $\tilde{S}_{\eta,1}^*$ and $\tilde{S}_{\eta,2}^*$. Equivalently, we also obtain two disjoint subsets $S_{\eta,1}^*$ and $S_{\eta,2}^*$ in the original manifold space, resulting in dividing D_η into

$$\begin{aligned} D_{\eta,1}^* &= \{(x^*, \mathbf{s}^*) \in D_\eta^* : \mathbf{s}^* \in S_{\eta,1}^*\} \\ D_{\eta,2}^* &= D_\eta^* \setminus D_{\eta,1}^*. \end{aligned}$$

3.2 An adaptive Soft semi-multivariate decision rule model

Given the recursive bipartition of the reference knots and a data point \mathbf{d} , we assume that the decision of assigning a data point \mathbf{d} to one of the two children nodes is a mixture of hard and soft decisions with different levels of smoothness, and the decision rule under each type of decision is a function depending on the distance of \mathbf{d} to its nearest reference knots in the two children nodes. This mixed decision-making allows us to capture both sharp changes and smooth variations in the regression tree function.

Let $A_\eta^{(h)}$ denote the type of decision at node η , taking values from $0, 1, \dots, k$. We associate a hard decision with node η if $A_\eta^{(h)} = 0$ such that \mathbf{d} is assigned to the left or right with probability 1. When $A_\eta^{(h)} \in \{1, \dots, k\}$, a soft decision is adopted at node η so that \mathbf{d} is either assigned to the left or right child with certain probabilities. We assume that $A_\eta^{(h)}$ follows a categorical prior distribution and is independent across internal nodes. Specifically, $A_\eta^{(h)} = \text{Categorical}(p_0, p_1, \dots, p_k)$, where $p_0 + \sum_{i=1}^k p_i = 1$.

Let $z_{\eta L}^{(h)}(\mathbf{d}) | (A_\eta^{(h)} = c)$ denote the decision rule function, i.e., the probability of \mathbf{d} going left when the c -th type of decision is adopted. Let $d_{\eta L}^{(h)}(\mathbf{d})$ and $d_{\eta R}^{(h)}(\mathbf{d})$ denote the distances between \mathbf{d} and the nearest knots assigned to the left and right children on the space of features used for splitting η , respectively (see Sections 2 and 3.1). It is reasonable to assume that when $d_{\eta L}^{(h)}(\mathbf{d}) < d_{\eta R}^{(h)}(\mathbf{d})$, \mathbf{d} is more likely to belong to the left child node. Therefore, we assume $z_{\eta L}^{(h)}(\mathbf{d}) | (A_\eta^{(h)} = c)$ is a monotone function of $d_{\eta R}^{(h)} - d_{\eta L}^{(h)}$.

In the hard case, we assume

$$z_{\eta L}^{(h)}(\mathbf{d}) | (A_\eta^{(h)} = 0) = \begin{cases} 1, & \text{if } d_{\eta L}^{(h)}(\mathbf{d}) \leq d_{\eta R}^{(h)}(\mathbf{d}) \\ 0, & \text{otherwise} \end{cases}$$

In the soft case, we introduce a monotone logistic gate function with scaling parameters to transform $d_{\eta R}^{(h)} - d_{\eta L}^{(h)}$ to a value in $[0, 1]$ as follows

$$\begin{aligned} z_{\eta L}^{(h)}(\mathbf{d}) | (A_\eta^{(h)} = c) &= \frac{1}{1 + e^{-\alpha_c^{(h)} \frac{d_{\eta R}^{(h)}(\mathbf{d}) - d_{\eta L}^{(h)}(\mathbf{d})}{C_\eta^{(h)}}}} \\ z_{\eta R}^{(h)}(\mathbf{d}) | (A_\eta^{(h)} = c) &= 1 - z_{\eta L}^{(h)}(\mathbf{d}) | (A_\eta^{(h)} = c) \end{aligned}$$

where $C_\eta^{(h)}$ is the maximum of the distances from the nearest left and right knots over all observations introduced to normalize the distances to make them unit-free, and $\alpha_c^{(h)}$ is a decision-specific

and tree-specific softness control parameter that scales the normalized distance adaptive to different decisions. The smaller the value of α , the smoother the decision boundary.

We consider two approaches to model the soft case as follows.

Approach 1. In this case, we only consider one soft decision type, i.e., $k = 1$, and we shall refer to this approach as S2-BAMDT. We also drop the subscript from $\alpha_1^{(h)}$ for notation simplicity. We treat $\alpha^{(h)}$ as a positive continuous random variable distinct for each tree and shall describe its prior model in Section 3.3. It follows that

$$z_{\eta L}^{(h)}(\mathbf{d})|(A_{\eta}^{(h)} = 1) = \frac{1}{1 + e^{-\alpha^{(h)} \frac{d_{\eta R}^{(h)}(\mathbf{d}) - d_{\eta L}^{(h)}(\mathbf{d})}{C_{\eta}^{(h)}}}}.$$

This approach requires all the internal nodes of the same tree to have the same smoothness level if their decisions are soft. However, we allow each tree to learn its distinct smoothness control parameter $\alpha^{(h)}$ to raise the additive model’s flexibility in capturing functions with different levels of smoothness. This way of introducing softness by tree-specific smoothness control parameters resembles that of the soft BART method in Linero and Yang [2018]. However, we emphasize that a key distinction of our approach is the ability to learn a node-specific decision in each tree, allowing some internal nodes to have hard decisions instead of imposing a soft decision rule for all nodes. Another important distinction between our approach and Linero and Yang [2018] is that we account for both structured and unstructured features, and we use knot sets at each branch to calculate the distance from each observation and find the probabilities of going left and right at each internal node.

Approach 2. In this case, we assume the soft decision at each node is chosen from a set of soft decisions with different levels of smoothness control parameters $\{\alpha_1^{(h)}, \dots, \alpha_k^{(h)}\}$, and we refer to this method as Sk-BAMDT. Unlike S2-BADMT, which uses a common smoothness control parameter for the entire tree and relies on varying it to adapt to different smoothness levels, Sk-BAMDT allows for node-specific decisions with varying smoothness control parameters. This enables the model to better adapt to varying smoothness even within a single tree. Moreover, the shallow depth of the trees limits the information available to infer the posterior of $\alpha_c^{(h)}$ especially for higher values of k . Therefore, we recommend fixing $\{\alpha_1^{(h)}, \dots, \alpha_k^{(h)}\}$ at a small discrete set of values $\{\alpha_1, \dots, \alpha_k\}$ that are common across all trees. It follows that

$$z_{\eta L}^{(h)}(\mathbf{d})|(A_{\eta}^{(h)} = c) = \frac{1}{1 + e^{-\alpha_c^{(h)} \frac{d_{\eta R}^{(h)}(\mathbf{d}) - d_{\eta L}^{(h)}(\mathbf{d})}{C_{\eta}^{(h)}}}}, \text{ for } c = 1, \dots, k.$$

Compared to Sk-BAMDT, which is sensitive to improperly pre-established smoothness levels, S2-BAMDT is less sensitive to the starting value of the smoothness level per tree.

Figure 1 compares hard and soft decision trees as derived by Linero and Yang [2018] (SBART) and the hard-soft decision trees of Sk-BAMDT and S2-BAMDT. Sk-BAMDT and S2-BAMDT are two distinct methods for generating hard-soft decision trees that adhere to boundary restrictions and inherent geometry, as seen in figure 1. In contrast to the single smoothness level applied in S2-BAMDT, the soft boundaries of Sk-BAMDT are determined by two distinct levels of smoothness.

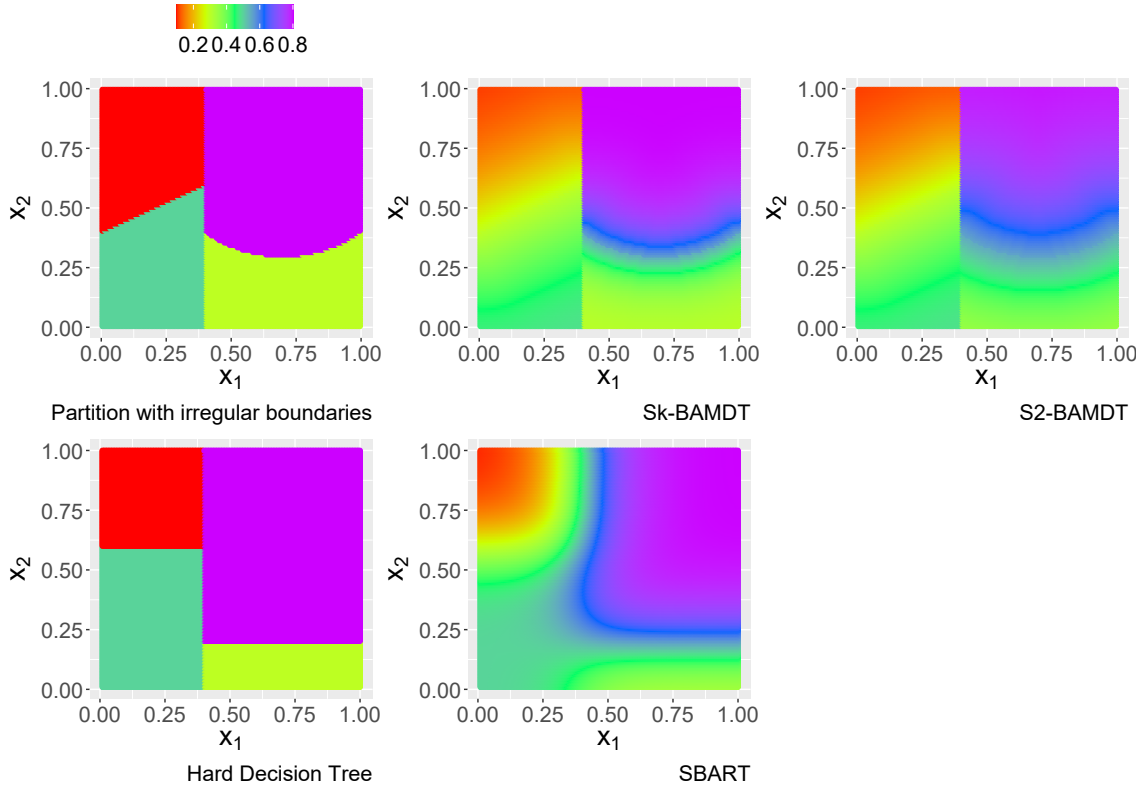


Figure 2: Comparison of a hard decision tree to a soft decision tree as derived by Linero (SBART) and the hard-soft decision trees of Sk-BAMDT and S2-BAMDT. We have used a logistic function with a bandwidth parameter equal to 0.08 for SBART, $\{\alpha_1, \alpha_2\} \times q = \{0.5, 1\} \times 12$ for Sk-BAMDT, and $\alpha^{(h)} \times q = 0.5 \times 12$ for S2-BAMDT.

Conditional on all the internal node decisions $\mathbf{A}^{(h)} := \{A_\eta^{(h)}\}_{\eta \in T^{(h)}}$ of the h -th decision tree $T^{(h)}$, the probability of a data point \mathbf{d} falling into the terminal node l is given by going down the probabilistic decision path of $T^{(h)}$,

$$\Phi_{hl}(\mathbf{d}) | \mathbf{A}^{(h)} = \prod_{\eta \in P_{hl}(\mathbf{d})} [z_{\eta L}^{(h)}(\mathbf{d}) | A_\eta^{(h)}] \mathbb{1}^{(r_{\eta L}^{(h)}=1)} (1 - [z_{\eta L}^{(h)}(\mathbf{d}) | A_\eta^{(h)}])^{1 - \mathbb{1}^{(r_{\eta L}^{(h)}=1)}}, \quad (2)$$

where $P_{hl}(\mathbf{d})$ is the path from the root to the terminal node l , $\mathbb{1}(\cdot)$ denotes the indicator function, $r_{\eta L}^{(h)}(\mathbf{d})$ is a binary variable with $r_{\eta L}^{(h)}(\mathbf{d}) = 1$ if the path goes left at node η .

Finally, the additive decision trees model takes the form,

$$f(\mathbf{d}) = \sum_{h=1}^m g(\mathbf{d}; T^{(h)}, \mathbf{M}^{(h)}) = \sum_{h=1}^m \sum_{l=1}^{L_h} \mu_{hl} \Phi_{hl}(\mathbf{d}), \quad (3)$$

where the value of each decision tree function is the probability-weighted average of leaf weights.

3.3 Priors of other model parameters.

Given a fixed number of trees, m , the parameters of the model are the tree components, $(\mathbf{T}, \mathbf{M}) = \{T^{(h)}, \mathbf{M}^{(h)}\}_{h=1}^m$, the control parameters $\boldsymbol{\alpha}$, the probabilistic decisions at each internal node, $\mathbf{A} =$

$\{\mathbf{A}^{(h)}\}_{h=1}^m$, the corresponding event probabilities parameters $\mathbf{p}_A = (p_0, p_1, \dots, p_k)$ in the categorical distribution for \mathbf{A} , the residual variance, σ^2 , and the leaf parameter variance, σ_μ^2 .

Following Chipman et al. [2010], we assume that the tree components are independent of each other and that the terminal node parameters of every tree are independent, so that the prior can be factorized as:

$$P(\mathbf{T}, \mathbf{M}, \mathbf{A}, \boldsymbol{\alpha}, \mathbf{p}_A, \sigma^2, \sigma_\mu^2) = \left(\prod_h P(T^{(h)}) \prod_\eta P(\mu_{h\eta} | T^{(h)}) P(A_\eta^{(h)} | \mathbf{p}_A, T^{(h)}, \boldsymbol{\alpha}) \right) \times P(\boldsymbol{\alpha}) P(\mathbf{p}_A) P(\sigma^2) P(\sigma_\mu^2).$$

3.3.0.1 Prior on the probabilistic decisions at internal nodes. We use a categorical prior distribution to model the probabilistic decisions \mathbf{A} whose event probabilities follows the following prior distribution

$$\mathbf{p}_A \sim \text{Dirichlet}(\boldsymbol{\psi}), \quad \boldsymbol{\psi} = (\psi_0, \psi_1, \dots, \psi_k), \quad \psi_0, \dots, \psi_k > 0,$$

We suggest $\boldsymbol{\psi} = (1, \dots, 1)$ as the default option in Sk-BADMT which works well in our numerical studies. In S2-BADMT with only two decisions, the categorical distribution is reduced to a Bernoulli distribution, and we assume a beta distribution prior to the probability of having a hard decision. We use Beta(1, 2) as the default choice in all our numerical studies.

3.3.0.2 Prior on the softness control parameter. These parameters allow us to appropriately rescale the normalized distance to adapt the probabilities $\{z_{\eta L}^{(h)}(\mathbf{d}) | A_\eta^{(h)} \neq 0\}$. Sk-BADMT assumes a fixed finite set of k values, $\boldsymbol{\alpha} = \{\alpha_1, \dots, \alpha_k\}$ corresponding to each soft category of $A_\eta^{(h)}$. In our numerical examples, we used $\{0.5, 1, 2\}$ times a positive constant $q \geq 1$ for $\boldsymbol{\alpha}$ while tuning the choice of q in different studies, which seems to work well in practice. Within the range of values between 1 and 13, we choose those values of the tuning parameter q that give the most accurate predictions based on Watanabe-Akaike information criterion [Gelman et al., 2014] and cross-validation [Gelman et al., 2014] for each simulation scenario. In S2-BADMT, we use a gamma distribution with shape α_g and rate β_g to model the control parameter, $\alpha^{(h)} \sim \text{Gamma}(\alpha_g, \beta_g)$. We set $\alpha_g = 1$ and $\beta_g = 0.5$ in our numerical studies.

3.3.0.3 Prior on the leaf weight parameters After rescaling Y into $[-0.5, 0.5]$, we use the conjugate normal distribution for μ_{hl} , conditional on $T^{(h)}$:

$$\mu_{hl} | T^{(h)}, \sigma_\mu^2 \sim \text{N}(0, \sigma_\mu^2), \quad \sigma_\mu^2 \sim \text{Inv-Gamma}(\alpha_\mu, \beta_\mu).$$

We apply an Inverse-Gamma prior to the variance of the leaf weight parameter, σ_μ^2 , following He and Hahn [2023], with hyperparameters $\alpha_\mu = 3$ and $\beta_\mu = 0.5 \times \text{Var}(y)/m$.

3.3.0.4 Prior on the residual variance In line with the original BART model [Chipman et al., 2010], we use a conjugate inverse- χ^2 prior for the residual variance, that is, $\sigma^2 \sim v\lambda/\chi_v^2$ for $v = 3$, and select λ , such that $P(\sigma^2 < \hat{\sigma}^2) = 0.90$ a priori, where $\hat{\sigma}^2$ is the sample variance of the responses.

3.3.0.5 Prior on the decision trees. Following Chipman et al. [2010], we adopt the Galton-Watson process [Harris et al., 1963] to model the tree prior for the recursive hard bipartitions of reference points. Each node has either zero or two offspring. The probability of splitting a node depends on its depth on the tree, taking the form:

$$p_{split}(\eta) = \frac{\gamma}{(1 + d(\eta))^\delta},$$

where $d(\eta)$ is the depth of node η in the tree. The hyper-parameters (γ, δ) control the shape of trees. The parameter $\gamma > 0$ controls the probability that the root of a tree will split into two offspring, while the parameter $\delta > 0$ penalizes against deep trees. As noted in Chipman et al. [2010], we want to keep the depth of the tree small whilst ensuring non-trivial trees. In our simulation study on real and synthetic data, we fix $\gamma = 0.95$ and $\delta = 2$.

If the node splits, we perform a multivariate split with probability p_m . Otherwise, we perform a univariate split. To perform a univariate split of D_η^* , we select uniformly one of the unstructured features, followed by a uniform selection from the available split values associated with that feature. We set $p_m = d_{\mathcal{M}}/(d_{\mathcal{M}} + p)$ where $d_{\mathcal{M}}$ is the dimensionality of the structured feature space \mathcal{M} and p is the number of unstructured features.

3.4 Connection between GP and the SBAMDT model

In this subsection, we explore the connection between SBAMDT and Gaussian processes (GPs) to reveal the behavior of decision tree models in capturing functional dependence and smoothness. As previously described, BART represents the latent regression function f as a summation of m decision tree piecewise constant functions. In this framework, the value produced by each tree is determined through a probability-weighted average of leaf weights, which depends on the decisions made at the internal nodes:

$$f(\mathbf{d}) = \sum_{h=1}^m g(\mathbf{d}; T^{(h)}, \mathbf{M}^{(h)}) = \sum_{h=1}^m \sum_{l=1}^{L_h} \mu_{hl} \phi_{hl}(\mathbf{d}),$$

where $\phi_{hl}(\mathbf{d})$ is defined as:

$$\phi_{hl}(\mathbf{d}) | \mathbf{A}^{(h)} = \prod_{\eta \in P_{hl}(\mathbf{d})} P_\eta(\mathbf{d}; A_\eta^{(h)}),$$

with the conditional probability given by:

$$P_\eta(\mathbf{d}; A_\eta^{(h)}) = [z_{\eta L}^{(h)}(\mathbf{d}) | A_\eta^{(h)}]^{\mathbb{1}(r_{\eta L}^{(h)}=1)} \left(1 - [z_{\eta L}^{(h)}(\mathbf{d}) | A_\eta^{(h)}]\right)^{1 - \mathbb{1}(r_{\eta L}^{(h)}=1)}.$$

Under the normal prior and posterior distributions for the leaf weight parameters, we present the following theorem, divided into two parts: the prior distribution and the posterior distribution.

Theorem 3.1 (Connection between SBAMDT and GP).

Prior distribution:

- (1) Conditional on \mathbf{T} and \mathbf{A} , the prior distribution of f is given by $f \sim GP(0, C(f_i, f_j))$, where the covariance function is determined by $C(f_i, f_j) = \frac{\beta_\mu}{\alpha_\mu - 1} \sum_{h=1}^m \sum_{l=1}^{L_h} \phi_{hl}(\mathbf{d}_i) \phi_{hl}(\mathbf{d}_j)$, and α_μ and β_μ are the hyperparameters of the Inverse-Gamma prior applied to the variance of the leaf-weight parameter. In the absence of hard splits, the process is mean square differentiable. However, if there is at least one hard split due to discontinuities in the indicator function, we cannot assert that the process is mean square differentiable overall.
- (2) Conditional on \mathbf{T} , the prior distribution of f is $f \sim GP(0, C(f_i, f_j))$ with the covariance matrix defined by $C(f_i, f_j) = \frac{\beta_\mu}{\alpha_\mu - 1} \sum_{h=1}^m \sum_{l=1}^{L_h} E(\phi_{hl}(\mathbf{d}_i) \phi_{hl}(\mathbf{d}_j))$, where the expectation is with respect to the distribution of \mathbf{A} , which holds in the limit as the number of trees approaches infinity. If there is at least one hard split, the process is not mean square differentiable everywhere.

Posterior Distribution:

- (1) We denote with $\{\hat{\mathbf{T}}, \hat{\mathbf{M}}, \hat{\mathbf{A}}, \hat{\sigma}^2, \hat{\sigma}_\mu^2\}$ the posterior sample of $\{\mathbf{T}, \mathbf{M}, \mathbf{A}, \sigma^2, \sigma_\mu^2\}$. Given $\{\hat{\mathbf{T}}, \hat{\mathbf{M}}^{(-h)}, \hat{\mathbf{A}}, \hat{\sigma}^2, \hat{\sigma}_\mu^2\}$, the distribution of the latent regression function $f(\mathbf{d})$ is a valid Gaussian process with a mean given by $\hat{\mu}_f^{(h)}(\mathbf{d}) = \hat{\mu}^{(h)T} \hat{\Phi}^{(h)}(\mathbf{d}) + \sum_{h'=1, h' \neq h}^m \hat{\mathbf{M}}^{(h')T} \hat{\Phi}^{(h')}(\mathbf{d})$ and a covariance function given by $\hat{C}(f_i, f_j) = \hat{\Phi}^{(h)T}(\mathbf{d}_i) \Omega^{(h)} \hat{\Phi}^{(h)}(\mathbf{d}_j)$, where $\hat{\Phi}^{(h)}(\mathbf{d}) = (\phi_{h1}(\mathbf{d}), \dots, \phi_{hL_h}(\mathbf{d}))^T$, where $\hat{\mu}^{(h)}$ and $\Omega^{(h)}$ are the mean and covariance matrix of the conditional distribution of $M^{(h)}$ that is a multivariate Gaussian distribution.
- (2) We denote with $\{\hat{\mathbf{T}}, \hat{\mathbf{M}}, \hat{\mathbf{A}}, \hat{\sigma}^2, \hat{\sigma}_\mu^2\}$ the posterior sample of $\{\mathbf{T}, \mathbf{M}, \mathbf{A}, \sigma^2, \sigma_\mu^2\}$. Given $\{\hat{\mathbf{T}}, \hat{\mathbf{A}}, \hat{\sigma}^2, \hat{\sigma}_\mu^2\}$, the posterior distribution of the latent regression function $f(\mathbf{d})$ is a valid Gaussian process with a mean given by $\hat{\mu}_f(\mathbf{d}) = \sum_{h=1}^m E(M^{(h)})^T \hat{\Phi}^{(h)}(\mathbf{d})$ and a covariance function given by $\hat{C}(f_i, f_j) = \sum_{h=1}^m \sum_{h'=1}^m \hat{\Phi}^{(h)T}(\mathbf{d}_i) C(M^{(h)}, M^{(h')}) \hat{\Phi}^{(h')}(\mathbf{d}_j)$, where $\hat{\Phi}^{(h)}(\mathbf{d}) = (\phi_{h1}(\mathbf{d}), \dots, \phi_{hL_h}(\mathbf{d}))^T$.

Proof. Appendix L includes the proof of Theorem 3.1. □

Building on Theorem 3.1, we further explore a specific hierarchical prior construction of decision trees based on the number of leaves, tree structures, and decision rules. The following proposition outlines the behavior of the resulting stochastic process of the latent regression function.

Proposition 3.2. Consider a hierarchical prior in which a shifted Poisson distribution is placed on the number of leaves, $P(L_h = k) = \frac{e^{-\lambda} \lambda^{k-1}}{(k-1)!}$, $k = 1, 2, 3, \dots$, and conditional on L_h , a uniform distribution on the tree structures with L_h leaves. We denote with $R^{(h)}$ the set of decision rules in $T^{(h)}$. Conditional on $T^{(h)}$ and L_h , the distribution of $R^{(h)}$ is given by the product rule probabilities, $P(R^{(h)} | T^{(h)}, L_h) = \prod_{\eta \in T^{(h)}} p_{rule}(\eta)$, where $p_{rule}(\eta)$ is the probability of the decision rule for node η . Then, $f \sim GP(0, C(f_i, f_j))$ with $C(f_i, f_j) = \frac{\beta_\mu}{\alpha_\mu - 1} \sum_{h=1}^m \sum_{k=1}^{\infty} P(L_h = k) P(T^{(h)} | L_h = k) P(R^{(h)} | T^{(h)}) \sum_{l=1}^k E(\phi_{hl}(\mathbf{d}_i) \phi_{hl}(\mathbf{d}_j))$ as $m \rightarrow \infty$.

With the foundation established in Theorem 3.1 and the subsequent Proposition 3.2, we can now contrast our SBAMDT model with the XBART-GP strategy developed by Wang et al. [2024]. While XBART-GP fits a Gaussian process at each leaf node of a BART tree and utilizes a squared exponential kernel to define the covariance function achieve a smooth stochastic process for prediction, our SBAMDT model naturally provides a globally valid stochastic process and hence a coherent framework for model estimation and prediction. SBAMDT does not require strong parametric assumptions on the covariance matrix. Instead, it quantifies the relative similarity between data points by multiplying their probabilities of falling into the same leaf and summing these products across all tree structures. The posterior covariance matrix of f involves the posterior of decision trees, making it nonstationary and highly adaptive. This allows SBAMDT to capture the complex relationships in the data more effectively than the XBART-GP method, which relies on predefined distance metrics.

4 Inference algorithm

We summarize our Bayesian hierarchical model below

$$\begin{aligned}
Y &= f(\mathbf{d}) + \epsilon, \quad \epsilon \stackrel{\text{iid}}{\sim} \text{N}(0, \sigma^2), \quad \mathbf{d} = (\mathbf{s}, \mathbf{x}) \\
f(\mathbf{d}) &= \sum_{h=1}^m \sum_{l=1}^{L_h} \mu_{hl} \phi_{hl}(\mathbf{d}) \\
\phi_{hl}(\mathbf{d}) | \mathbf{A}^{(h)} &= \prod_{\eta \in P_{hl}(\mathbf{d})} [z_{\eta L}^{(h)}(\mathbf{d}) | A_{\eta}^{(h)}]^{1(r_{\eta L}^{(h)}=1)} (1 - [z_{\eta L}^{(h)}(\mathbf{d}) | A_{\eta}^{(h)}])^{1-1(r_{\eta L}^{(h)}=1)} \\
\mu_{hl} | (T^{(h)}, \sigma_{\mu}^2) &\stackrel{\text{iid}}{\sim} \text{N}(0, \sigma_{\mu}^2), \quad \sigma_{\mu}^2 \sim \text{Inv-Gamma}(\alpha_{\mu}, \beta_{\mu}), \quad \sigma^2 \sim \frac{v\lambda}{\chi_v^2}, \\
T^{(h)} &\sim \text{Galton-Watson process}
\end{aligned}$$

Approach 1:

$$\begin{aligned}
A_{\eta}^{(h)} | \mathbf{p}_A &\sim \text{Multinomial}(\mathbf{p}_A), \quad \mathbf{p}_A = (p_0, p_2, \dots, p_k), \quad \sum_{i=1}^k p_i = 1 - p_0 \\
\mathbf{p}_A &\sim \text{Dirichlet}(\boldsymbol{\psi}), \quad \boldsymbol{\psi} = (\psi_0, \dots, \psi_k), \quad \psi_0, \dots, \psi_k > 0.
\end{aligned}$$

Approach 2:

$$\begin{aligned}
a^{(h)} &\sim \text{Gamma}(a_g, \beta_g) \\
A_{\eta}^{(h)} | p_A &= \begin{cases} 1 \text{ (hard)} & \text{wp } p_A \\ 0 \text{ (soft)} & \text{wp } 1 - p_A \end{cases} \\
p_A &\sim \text{Beta}(s_a, s_b).
\end{aligned}$$

We describe the Bayesian inference algorithm for Sk-BAMDT and defer the detailed algorithm for S2-BAMDT to Appendix J. Given the observed data $\mathbf{Y} = \{Y_i\}_{i=1}^n$, we seek to draw posterior samples of the model parameters $(\mathbf{T}, \mathbf{M}, \mathbf{A}, \mathbf{p}_A, \sigma^2, \sigma_{\mu}^2)$ from their posterior distributions.

For any arbitrary tree $T^{(h)}$, let us denote the set of the remaining trees as $T^{(-h)} = \{T_j\}_{j \neq h}$ whose associated leaf parameters are denoted as $\mathbf{M}^{(-h)}$ and node probabilistic decisions are denoted as

$\mathbf{A}^{(-h)}$. Let $\mathbf{R}^{(h)} = \mathbf{Y} - \sum_{j \neq h} g(\mathbf{d}; T^{(j)}, \mathbf{M}^{(j)})$ denote the residual response data conditional on other decision trees. We follow the backfitting Markov chain Monte Carlo (MCMC) sampler [Hastie and Tibshirani, 2000] to draw each decision tree parameters $(T^{(h)}, \mathbf{M}^{(h)}, \mathbf{A}^{(h)})$ from their respective full conditional distributions of global model parameters $(\mathbf{p}_A, \sigma^2, \sigma_\mu^2)$ and other local decision tree specific parameters, $(T^{(-h)}, \mathbf{M}^{(-h)}, \mathbf{A}^{(-h)})$ as shown in Algorithm 1.

A draw from $T^{(h)}, \mathbf{M}^{(h)}, \mathbf{A}^{(h)} | T^{(-h)}, \mathbf{M}^{(-h)}, \mathbf{A}^{(-h)}, \sigma^2, \sigma_\mu^2, \mathbf{p}_A, Y$ is equivalent to a draw from $T^{(h)}, \mathbf{M}^{(h)}, \mathbf{A}^{(h)} | \mathbf{R}^{(h)}, \sigma^2, \sigma_\mu^2, \mathbf{p}_A$. A draw from $T^{(h)}, \mathbf{M}^{(h)}, \mathbf{A}^{(h)} | \mathbf{R}^{(h)}, \sigma^2, \sigma_\mu^2, \mathbf{p}_A$ is equivalent to a draw from $T^{(h)} | \mathbf{R}^{(h)}, \sigma^2, \sigma_\mu^2, \mathbf{p}_A, Y$ followed by a draw from $\mathbf{A}^{(h)} | T^{(h)}, \mathbf{R}^{(h)}, \sigma^2, \sigma_\mu^2, \mathbf{p}_A$ and a draw from $\mathbf{M}^{(h)} | T^{(h)}, \mathbf{A}^{(h)}, \mathbf{R}^{(h)}, \sigma^2, \sigma_\mu^2$.

We propose a Metropolis-Hastings Algorithm to sample from

$$P(T^{(h)} | \mathbf{R}^{(h)}, \mathbf{A}^{(h)}, \sigma^2, \sigma_\mu^2) \propto P(\mathbf{R}^{(h)} | T^{(h)}, \mathbf{A}^{(h)}, \sigma^2, \sigma_\mu^2) P(T^{(h)}).$$

The transition kernel is chosen among the three proposals: GROW, PRUNE, and CHANGE. The GROW proposal randomly picks a terminal node, splits the chosen terminal into two new nodes, and assigns a decision rule to it. The PRUNE proposal randomly picks a parent of two terminal nodes and turns it into a terminal node by collapsing the nodes below it. The CHANGE proposal randomly picks an internal node and randomly reassigns to it a probabilistic decision. We describe the implementation of the proposals in Appendix I. In our simulation study, the probabilities of the proposals are set to: $P(\text{GROW}) = P(\text{PRUNE}) = 0.4$, and $P(\text{CHANGE}) = 0.2$.

Then, we have the following results required for the implementation of Algorithm 1.

1. The conditional likelihood is given by

$$P(\mathbf{R}^{(h)} | \mathbf{M}^{(h)}, T^{(h)}, \mathbf{A}^{(h)}, \sigma^2) = \prod_{i=1}^n (2\pi\sigma^2)^{-1/2} \exp\left(-\frac{1}{2\sigma^2} \left(R_i^{(h)} - \sum_{l=1}^{L_h} \mu_{hl} \phi_{hl}(\mathbf{d}_i)\right)^2\right). \quad (4)$$

2. The conditional integrated likelihood is given by

$$P(\mathbf{R}^{(h)} | T^{(h)}, \mathbf{A}^{(h)}, \sigma^2, \sigma_\mu^2) = \frac{|2\pi\Omega|^{1/2}}{(2\pi\sigma^2)^{n/2} |2\pi\sigma^2 I|^{1/2}} \exp\left(-\frac{\|\mathbf{R}^{(h)}\|^2}{2\sigma^2} + \frac{1}{2} \hat{\boldsymbol{\mu}}^T \Omega^{-1} \hat{\boldsymbol{\mu}}\right), \quad (5)$$

where

$$\hat{\boldsymbol{\mu}} = \Omega \sum_{i=1}^n \frac{R_i^{(h)} \boldsymbol{\Phi}_i}{\sigma^2}, \quad \Omega^{-1} = \left(\frac{I}{\sigma_\mu^2} + \Lambda\right), \quad \Lambda = \frac{1}{\sigma^2} \sum_{i=1}^n \boldsymbol{\Phi}_i \boldsymbol{\Phi}_i^T, \quad \boldsymbol{\Phi}_i^T = (\phi_{h1}(\mathbf{d}_i), \dots, \phi_{hL_h}(\mathbf{d}_i)),$$

I the $L_h \times L_h$ identity matrix, $|U|$ the determinant of the matrix U and $\|z\|$ the Euclidean norm of vector z .

3. The conditional distribution of $\mathbf{M}^{(h)}$ is a multivariate Gaussian distribution with mean $\hat{\boldsymbol{\mu}}^{(h)}$ and covariance matrix $\Omega^{(h)}$:

$$\mathbf{M}^{(h)} | \mathbf{R}^{(h)}, T^{(h)}, \mathbf{A}^{(h)}, \sigma^2, \sigma_\mu^2 \sim N(\hat{\boldsymbol{\mu}}^{(h)}, \Omega^{(h)}).$$

4. The conditional distribution of σ^2 is an Inverse-gamma distribution with shape $s_{1\sigma} = \frac{n+v}{2}$ and scale $s_{2\sigma} = \frac{1}{2} \sum_{i=1}^n \left(Y_i - \sum_{h=1}^m \sum_{l=1}^{L_h} \mu_{hl} \phi_{hl}(\mathbf{d}_i)\right)^2 + \frac{v\lambda}{2}$.

5. The conditional distribution of σ_μ^2 is an Inverse-gamma distribution with shape $s_{1\mu} = \alpha_\mu + \frac{1}{2} \sum_{h=1}^m L_h$ and scale $s_{2\mu} = \frac{1}{2} \sum_{h=1}^m \sum_{l=1}^{L_h} \mu_{hl}^2 + \beta_\mu$.
6. The conditional distribution of \mathbf{p}_A is a Dirichlet distribution:

$$P(\mathbf{p}_A | \mathbf{T}, \mathbf{A}) \sim \text{Dirichlet}(\tilde{\boldsymbol{\psi}}), \quad \tilde{\boldsymbol{\psi}} = (\tilde{\psi}_0, \dots, \tilde{\psi}_k), \quad \tilde{\psi}_l = \sum_h \sum_\eta \mathbf{1}(A_\eta^{(h)} = l) + \psi_l.$$

7. The conditional distribution of $A_\eta^{(h)}$ is a Multinomial distribution :

$$A_\eta^{(h)} | T^{(h)}, \mathbf{p}_A, \mathbf{R}^{(h)}, \sigma^2, \sigma_\mu^2 \sim \text{Multinomial}(w_{Ah}), \quad w_{Ah} = (w_{h0}, \dots, w_{hk})$$

$$w_{hl} = \frac{p_l P(\mathbf{R}^{(h)} | T^{(h)}, A_\eta^{(h)} = l, \sigma^2, \sigma_\mu^2)}{\sum_{j=0}^k p_j P(\mathbf{R}^{(h)} | T^{(h)}, A_\eta^{(h)} = j, \sigma^2, \sigma_\mu^2)}.$$

The proof can be found in the appendix.

Algorithm 1 Metropolis-Hastings within Gibbs sampler (Sk-BAMDT)

```

for  $t = 1, 2, 3, \dots$  do
  for  $h = 1$  to  $m$  do
    Sample  $T^{(h)} | \mathbf{R}^{(h)}, \sigma^2, \sigma_\mu^2, \mathbf{p}_A$  using a Metropolis-Hastings Algorithm.
    If  $T^{(h)}$  grows, sample the probabilistic decision for the new internal node  $\eta$ ,
     $A_\eta^{(h)} | \mathbf{R}^{(h)}, T^{(h)}, \sigma^2, \sigma_\mu^2, \mathbf{p}_A$ , from  $\text{Multinomial}(w_{Ah})$ .
    Sample  $\mathbf{M}^{(h)} | \mathbf{R}^{(h)}, T^{(h)}, \mathbf{A}^{(h)}, \sigma^2, \sigma_\mu^2$  from  $\text{N}(\hat{\boldsymbol{\mu}}^{(h)}, \Omega^{(h)})$ .
  end for
  Sample  $\sigma^2 | \mathbf{T}, \mathbf{M}, \mathbf{A}, \mathbf{Y}$  from  $\text{Inverse-Gamma}(s_{1\sigma}, s_{2\sigma})$ .
  Sample  $\sigma_\mu^2 | \mathbf{T}, \mathbf{M}, \mathbf{A}, \mathbf{Y}$  from  $\text{Inverse-Gamma}(s_{1\mu}, s_{2\mu})$ .
  Sample  $\mathbf{p}_A | \mathbf{T}, \mathbf{A}$  from  $\text{Dirichlet}(\tilde{\boldsymbol{\psi}})$ .
end for

```

5 Simulation study on synthetic data

Using synthetic data, we show the effectiveness of our proposed SBAMDT models, namely Sk-BAMDT and S2-BAMDT. In addition to SBAMDT, we consider three benchmark additive decision tree models for comparisons, including BART [Chipman et al., 2010], SBART [Linero and Yang, 2018], and BAMDT [Luo et al., 2022]. We present two simulation scenarios in this section. The first has a rotated U-shaped domain with circular boundaries, where SBAMDT and BAMDT are particularly suitable. The second has a square domain with horizontal and vertical boundaries to examine the robustness of our method in a case that favors the competing methods, BART and SBART. See Appendix 2 for an additional simulation example where the true function is a piecewise Gaussian process on the U-shaped domain.

For each model, we employ $m = 30$ weak learners. For each unstructured feature, we utilize 100 equally spaced grid points as candidate split cutoff values. We discard the first 5000 iterations

as burn-in and apply thinning by retaining one sample every five iterations from the remaining 15000 iterations of the MCMC algorithms in SBAMDT, BAMDT and BART. For SBART, we discard the first 8000 iterations as burn-in and save 3000 samples after thinning.

We evaluate the prediction performance of SBAMDT and its competitors in terms of root mean square prediction error (RMSPE), mean absolute prediction error (MAPE), and continuous ranked probability score [CRPS, Gneiting and Raftery, 2007]. For all metrics, lower values indicate better performance.

5.1 U-shape Example

We consider a 45-degree rotation of a U-shaped domain using longitude and latitude as structural features. A 0.9-radius circle centred at the origin divides the U-shaped domain into three clusters. We generate ten unstructured features where each feature is an independent realisation from a Gaussian process on the U-shape domain. We use a training data set of size $n = 500$, a test data set of size $n_{test} = 200$, and a piecewise smooth function dependent on (\mathbf{s}, x_1) and their interaction. See Figure 3 for an illustration of the true function and the domain. With a noise level of $\sigma = 0.1$, we generate 50 response replicates in the training and test data from Equation (1). A random subset of 100 training data is employed as knots for BAMDT and SBAMDT.

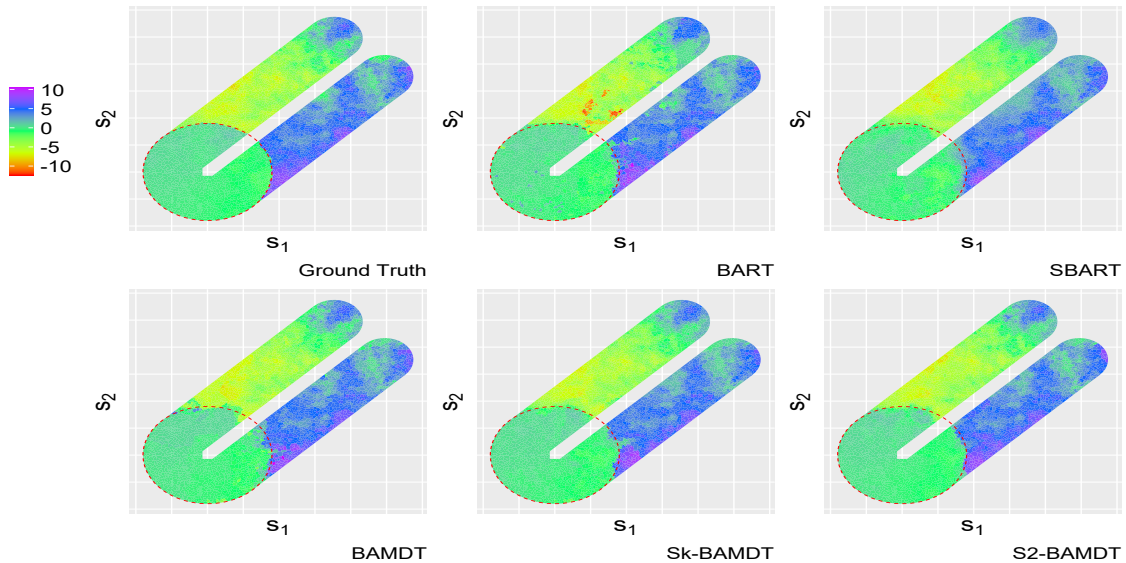


Figure 3: The ground truth for $f(\mathbf{s}, \mathbf{x})$ and the predictive surfaces $\hat{f}(\mathbf{s}, \mathbf{x})$ of each method for a U-shape simulated data. The red circle indicates discontinuity boundaries in the true function projected to the 2-D U-shape domain.

Table 1: **U-shape**. The average performance metrics and their standard deviations (in parenthesis) for SBAMDT and benchmark models over 50 replicates.

	SBAMDT and Benchmark models				
	BAMDT	BART	SBART	Sk-BAMDT (q=8)	S2-BAMDT (q=8)
MAPE $\times 10^{-1}$	4.88(0.53)	7.09(0.48)	6.36(0.29)	3.93(0.43)	4.13(0.72)
RMSPE $\times 10^{-1}$	10.01(1.29)	12.52(1.00)	10.18(0.38)	9.14(0.77)	9.73(1.22)
CRPS $\times 10^{-1}$	4.00(0.50)	5.85(0.45)	4.70(0.19)	3.03(0.32)	3.24(0.47)

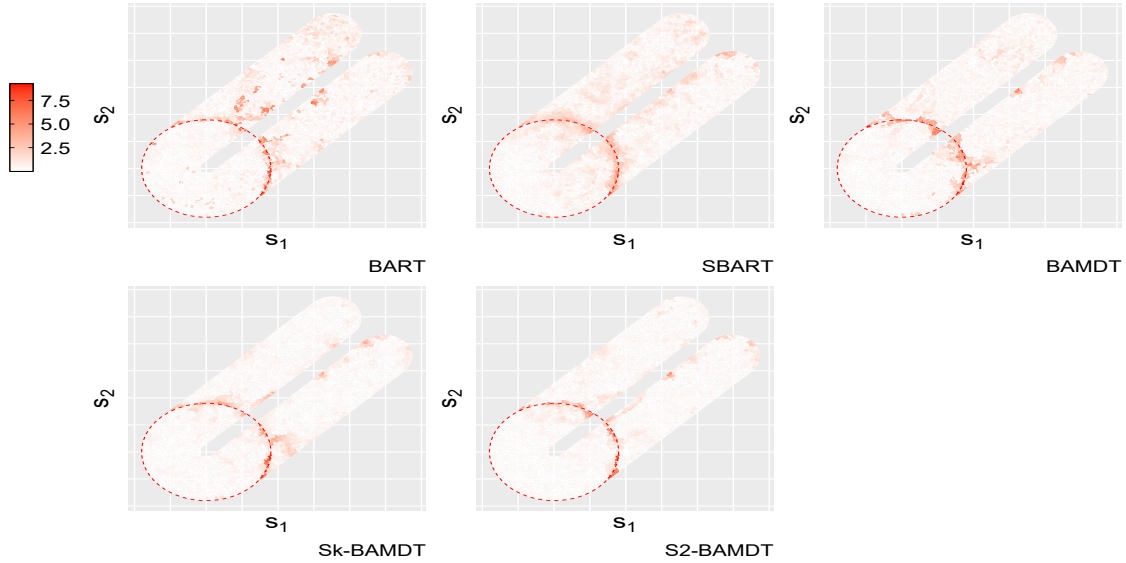


Figure 4: The APE of each method for one U-shape simulation.

Table 1 summarizes the average performance metrics of the benchmark models and SBAMDT over 50 replicates, demonstrating that Sk-BAMDT performs the best among these methods, followed by S2-BADMT and BAMDT. The SBAMDT and BAMDT models outperform BART and SBART due to the use of multivariate splits that can more flexibly handle circular-shaped function discontinuities and U-shape complex domains. The win of SBAMDT over BAMDT illustrates the need to consider soft splits of the feature space by employing probabilistic decisions at decision tree internal nodes, which enables SBAMDT to better approximate functions with adaptive smoothness inside each cluster.

Figures 3, 4 and 5 display the mean predictive surfaces, absolute prediction error (APE) and CRPS from SBAMDT and benchmark models for one randomly selected experiment, respectively. These figures again confirm that, in general, SBAMDT provides the best fit to the ground truth at most locations with smaller errors both around the circular jump and in the interior of the clusters. In contrast, BART and SBART suffer from some axis-parallel artifacts especially near the circular jump boundary. We also notice that BART and SBART have large errors at many locations near the domain boundaries separating the lower and upper arms of U-shape, mainly due to the fact that axis-parallel split could group two regions separated by physical barriers into one cluster.

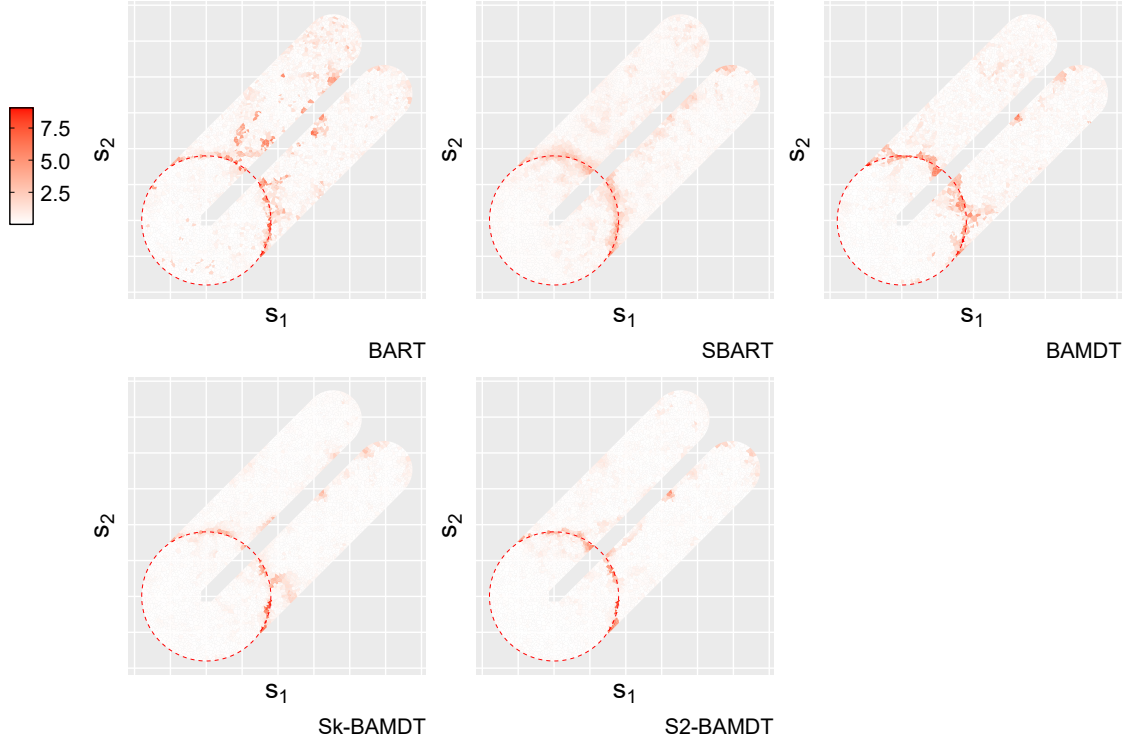


Figure 5: The CRPS of SBAMDT, BAMDT, BART and SBART associated with U-shape Example.

Moreover, it is evident from these figures that SBAMDT successfully reduces the prediction errors inside the clusters compared with BAMDT.

The additive decision tree models provide feature’s importance by taking the posterior mean of how many times the feature occurs in the ensemble of trees, which we also include as a metric for model comparison. Figure 17 shows the significance metric for both structured and unstructured features for all models using one of the fifty simulated data sets. The analysis demonstrates that all methods are capable of identifying important features, x_1 and \mathbf{s} . SBART performs better in identifying noisy features since it applies a Dirichlet prior to the splitting probability proportion of features.

5.2 2-D Square Example

We now examine the performance of SBAMDT in a scenario on a simple square domain with horizontal and vertical jumps, which aligns with the assumptions of BART and SBART and hence favors these two competing methods. Specifically, data is generated using a piecewise smooth function on $[0, 1]^2$ given by

$$f(\mathbf{d}) = \begin{cases} \sin(7x_1) \cos(4x_2) & \text{for } x_1 \geq 0, x_2 \leq 0 \\ 1 + \frac{2}{7}(2x_1 + 1)^2 + (2x_2 + 1)^2 & \text{for } x_1 \geq 0, x_2 > 0 \\ 5 & \text{for } x_1 < 0, x_2 \leq 0.2 \\ -5 & \text{for } x_1 < 0, x_2 > 0.2. \end{cases}$$

For simplicity, we consider a noise-free environment without adding irrelevant features. In the SBAMDT and BAMDT models, (x_1, x_2) is used as multivariate structural features, and each individual x is also included as a univariate unstructural feature. This approach enables the algorithm to detect function variations within each cluster where both features are necessary, while allowing each univariate feature to be used for identifying axis-parallel splits.

We use a training data set of size $n = 500$, a test data set of size $n_{test} = 200$ and repeat the experiments 50 times with a noise level $\sigma = 0.1$. A random subset of 140 training data is used as knots for SBAMDT and BAMDT.

The average performance metrics of Sk-BAMDT and the benchmark models over 50 replicates are summarised in Table 2. For one of the simulated data sets, Figures 6 and 7 display the absolute prediction error (APE) and mean predictive surfaces obtained from SBAMDT and benchmark models. While BART is favoured in this example, Sk-BAMDT outperforms its competitors. Sk-BAMDT performs better than BART because it can adjust to the function’s greater smoothness levels while taking into account a comparatively small number of trees. Sk-BAMDT’s win against SBART highlights our primary distinction: instead of enforcing a soft decision rule on every node, Sk-BAMDT permits some internal nodes to make hard decisions. Soft splits are required to adjust to greater smoothness levels of the regression function, as demonstrated by SBAMDT’s win against BAMDT.

Table 2: The average performance metrics for SBAMDT and benchmark models over 50 replicates. Numbers in parenthesis correspond to the standard deviation of the forecasts among the different replicates associated with Toy Example.

	SBAMDT and Benchmark models				
	BAMDT	BART	SBART	Sk-BAMDT (q=8)	S2-BAMDT (q=10)
MAPE $\times 10^{-1}$	3.46(0.46)	3.39(0.52)	5.87(0.41)	2.79(0.67)	3.06 (0.71)
RMSPE $\times 10^{-1}$	10.34(1.06)	10.76(1.39)	10.45(0.59)	9.54(3.76)	11.35 (3.46)
CRPS $\times 10^{-1}$	2.91(0.43)	2.79(0.48)	4.31(0.32)	2.14(0.65)	2.52 (0.68)

6 Application to NYC Education

In this section, we use online data from NYC Education (2000) [GeoDa Data and Lab] and apply SBAMDT and benchmark models (BAMDT, BART, SBART) to evaluate the predictive performance of SBAMDT. We model the logarithm of mean income as a function of the following variables: the total population under the age of eighteen (x_1); the percentage of all students enrolled in private schools (x_2); the percentage of the population aged sixteen to nineteen that has dropped out of high school (x_3); the percentage of the population aged twenty-five and over that has dropped out of high school (x_4); the percentage of the population aged twenty-five and over that has completed at least a bachelor’s degree (x_5); the number of schools (x_6) and the location of the population (in latitude and longitude). We treat the location as a structured feature (s_1 : longitude, s_2 : latitude) and all other covariates as unstructured features (\mathbf{x}).

The dataset comprises 1,690 entries, from which we selected 80% for training and 20% for testing. For the knots, a random selection of 420 training data points was used. We employed 100

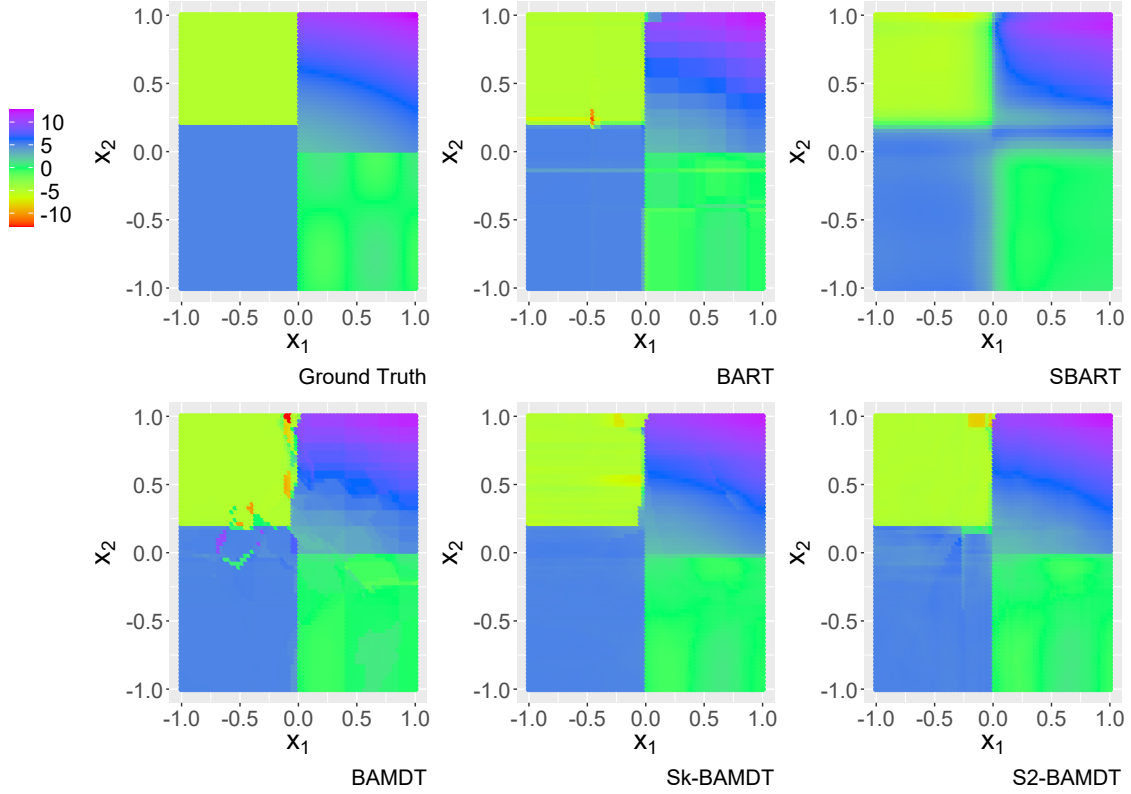


Figure 6: The ground truth for $f(\mathbf{s}, \mathbf{x})$ and the predictive surfaces $\hat{f}(\mathbf{s}, \mathbf{x})$ of SBAMDT, BAMDT, BART and SBART associated with Toy Example.

grid points as potential univariate split cutoff values for each unstructured feature and executed MCMC algorithms for 20,000 iterations, retaining every tenth sample after discarding the first 10,000 iterations as burn-in. For SBART, we similarly discarded the first 10,000 iterations and saved 1,000 samples after thinning.

Performance metrics in log scale, presented in Table 3, indicate that SBAMDT achieves superior predictive accuracy compared to its competitors. Figure 8 illustrates the fitted and observed income values at testing locations, demonstrating the model’s alignment with actual outcomes. Additionally, Figure 9 showcases the mean prediction surfaces of both SBAMDT and benchmark models across various locations, with unstructured features set at their median values. Key statistics include a population of 650.08 individuals under eighteen, 24% of students attending private schools, a high school dropout rate of 6.6% for those aged 16–19, a 26% dropout rate for individuals over 25, and 21% of this group holding at least a bachelor’s degree. Notably, the number of schools in the area is zero.

The comparison in Figure 9 reveals that while BAMDT and SBAMDT conform to boundary requirements, BART and SBART fail to capture spatial patterns, particularly in Manhattan. Some areas of the SBART predictive surface are overly smooth, obscuring spatial characteristics. BART divides the domain into hyperrectangular segments, identifying axis-parallel boundaries without flexibility. In contrast, SBAMDT and BAMDT recognize more adaptable borders through multivariate splits. SBAMDT achieves smoother patterns and improved predictions, particularly in the Belt Parkway area, due to soft splits and probabilistic decisions at internal nodes.

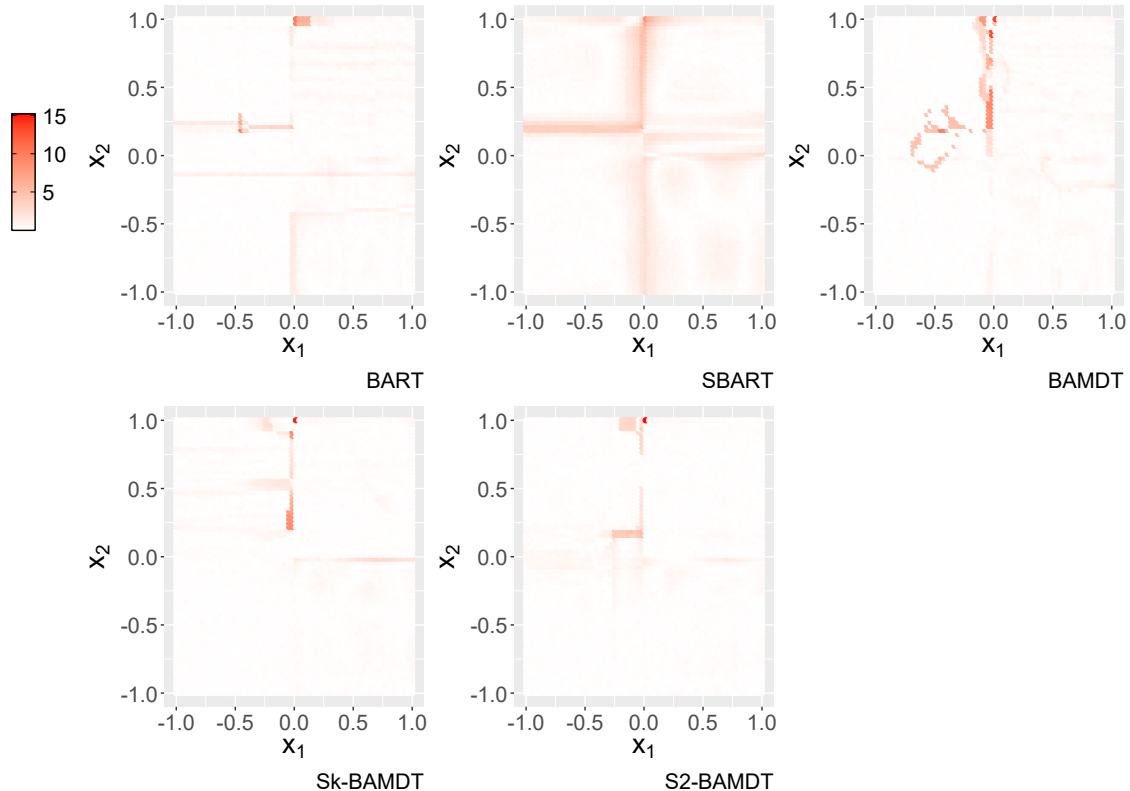


Figure 7: The APE of SBAMDT, BAMDT, BART and SBART associated with Toy Example.

Figure 15 presents the importance metrics for both structured and unstructured features across the models. Location emerges as the most significant determinant of income, followed by the number of schools (x_6) and the high school dropout rate for 16–19-year-olds (x_3). The differences in importance metrics between SBAMDT and BAMDT may stem from the softness control parameter, warranting further analysis in future work.

The population over 25 with at least a bachelor’s degree is identified as the second most significant factor by Sk-BAMDT, BAMDT, and BART. We analyze its impact in areas such as Woodside, Long Island City, Astoria, Corona, and John F. Kennedy International Airport by fixing other unstructured variables at their median values. Figure 16 depicts the marginal influence of higher educational attainment on income, showing a positive nonlinear relationship across regions, as anticipated. This effect varies by location, with individuals in Corona and Woodside earning more with higher education levels.

Table 3: The performance metrics for SBAMDT and benchmark models (NYC Education Data).

	Benchmark models				
	BAMDT	BART	SBART	Sk-BAMDT (q=10)	S2-BAMDT (q=6)
MAPE $\times 10^{-1}$	1.77	1.83	1.76	1.66	1.65
RMSPE $\times 10^{-1}$	3.05	3.25	3.09	2.96	2.85
CRPS $\times 10^{-1}$	1.49	1.54	1.50	1.34	1.32

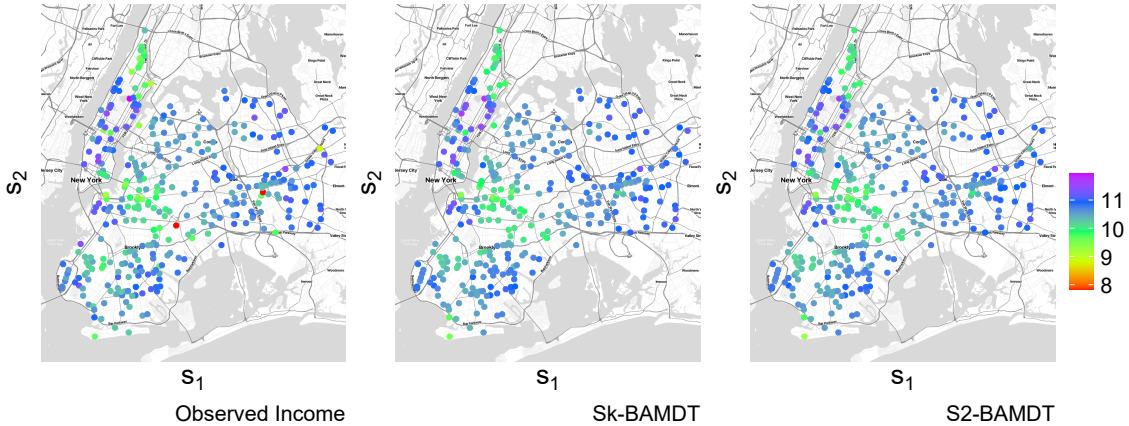


Figure 8: The observed and fitted value of income at observed locations for SBAMDT.

7 Conclusion

In this paper, we introduce SBAMDT, a novel Bayesian additive decision tree model designed to model nonparametric functions with both structured and unstructured features. By employing an adaptive decision rule that allows both hard and soft decisions at each internal node, SBAMDT facilitates rapid transitions and adaptive smooth changes, enhancing its flexibility in capturing complex data relationships. This model allows for node-specific decision-making and accommodates structured features through multivariate splits as well as unstructured features via univariate splits. Our extensive simulation studies using both synthetic and real datasets show that SBAMDT consistently outperforms BART, SBART, and BAMDT, highlighting its efficacy in diverse applications.

Future work could focus on several areas for improvement. First, optimizing the code for faster execution would enhance its usability for large datasets. Second, incorporating a Dirichlet prior for feature splitting probabilities may refine the model’s decision-making process further and improve its ability to handle higher dimensional features. Third, investigating the theoretical performance of function approximation through Bayesian posterior concentration theories could yield valuable insights into the model’s behavior. Lastly, expanding the application of SBAMDT beyond nonparametric regression to tasks such as classification and causal inference presents exciting opportunities for further research.

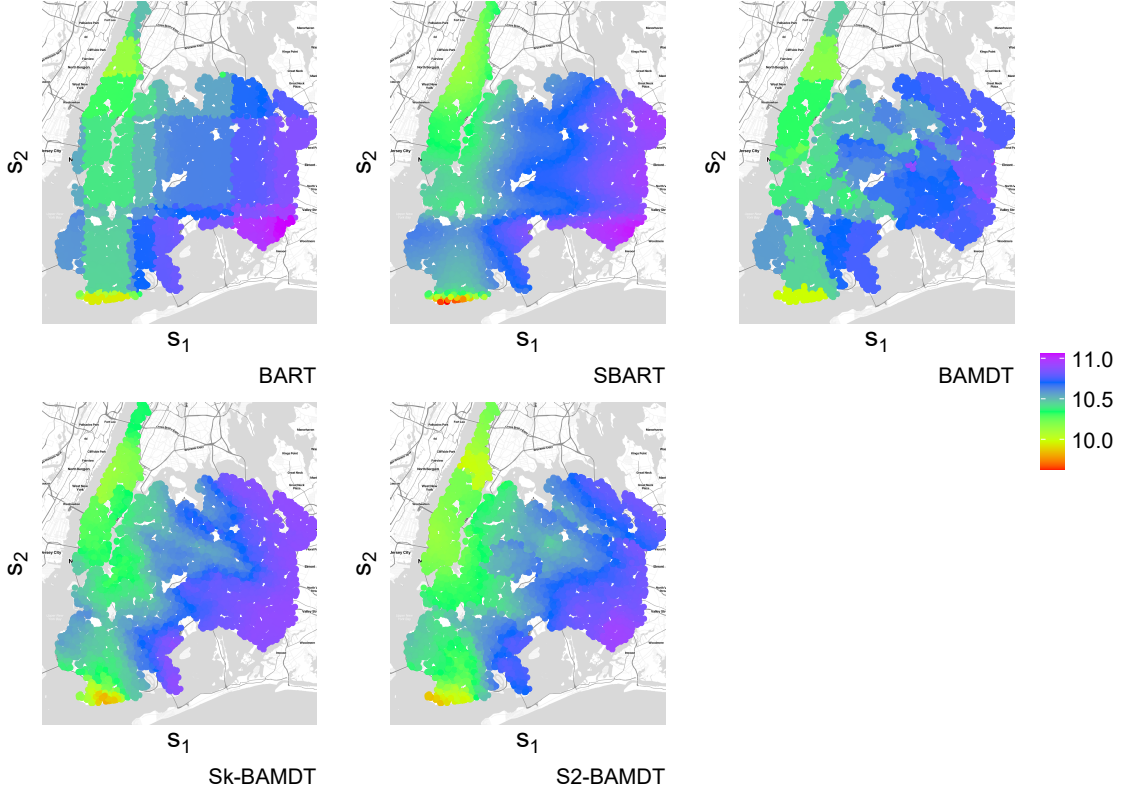


Figure 9: The spatial partial dependence plots for SBAMDT, BAMDT, BART, and SBART.

A The conditional integrated likelihood

It holds that

1.

$$P(\mathbf{R}^{(h)} | \mathbf{M}^{(h)}, T^{(h)}, \mathbf{A}^{(h)}, \sigma^2, \sigma_\mu^2) = (2\pi\sigma^2)^{-n/2} \times \prod_{i=1}^n \exp \left(-\frac{1}{2\sigma^2} \left(R_i^2 - 2R_i \sum_{l=1}^{L_h} \phi_{hl}(\mathbf{d}_i) \mu_{hl} + \left(\sum_{l=1}^{L_h} \phi_{hl}(\mathbf{d}_i) \mu_{hl} \right)^2 \right) \right)$$

2.

$$P(\mathbf{M}^{(h)} | T^{(h)}, \sigma_\mu^2) = |2\pi\sigma_\mu^2|^{-1/2} \exp \left(-\frac{1}{2} \mathbf{M}^{(h)T} \frac{1}{\sigma_\mu^2} \mathbf{I} \mathbf{M}^{(h)} \right)$$

3.

$$\left(\mathbf{M}^{(h)} - \Omega \frac{1}{\sigma^2} \sum_{i=1}^n \Phi_i R_i^{(h)} \right)^T \Omega^{-1} \left(\mathbf{M}^{(h)} - \Omega \frac{1}{\sigma^2} \sum_{i=1}^n \Phi_i R_i^{(h)} \right) = \mathbf{M}^{(h)T} \Omega^{-1} \mathbf{M}^{(h)} - \frac{2}{\sigma^2} \sum_{i=1}^n R_i^{(h)} \Phi_i^T \mathbf{M}^{(h)} + \hat{\boldsymbol{\mu}}^T \Omega^{-1} \hat{\boldsymbol{\mu}}$$

Thus, the conditional integrated likelihood is given by

$$\begin{aligned} P(\mathbf{R}^{(h)}|T^{(h)}, \mathbf{A}^{(h)}, \sigma^2, \sigma_\mu^2) &= (2\pi\sigma^2)^{-n/2} |2\pi\sigma_\mu^2 I|^{-1/2} \exp\left(-\frac{\|\mathbf{R}^{(h)}\|^2}{2\sigma^2}\right) \exp\left(\frac{1}{2}\hat{\boldsymbol{\mu}}^T \Omega^{-1} \hat{\boldsymbol{\mu}}\right) \times \\ &\quad \int \exp\left((\mathbf{M}^{(h)} - \hat{\boldsymbol{\mu}})^T \Omega^{-1} (\mathbf{M}^{(h)} - \hat{\boldsymbol{\mu}})\right) d\mathbf{M}^{(h)} \\ &= \frac{|2\pi\Omega|^{1/2}}{(2\pi\sigma^2)^{n/2} |2\pi\sigma_\mu^2 I|^{1/2}} \exp\left(-\frac{\|\mathbf{R}^{(h)}\|^2}{2\sigma^2} + \frac{1}{2}\hat{\boldsymbol{\mu}}^T \Omega^{-1} \hat{\boldsymbol{\mu}}\right). \end{aligned}$$

B The conditional distribution of $\mathbf{M}^{(h)}$

We have that

$$\begin{aligned} P(\mathbf{M}^{(h)}|T^{(h)}, \mathbf{A}^{(h)}, \mathbf{R}^{(h)}, \sigma^2, \sigma_\mu^2) &\propto P(\mathbf{R}^{(h)}|\mathbf{M}^{(h)}, T^{(h)}, \mathbf{A}^{(h)}, \mathbf{R}^{(h)}, \sigma^2, \sigma_\mu^2) P(\mathbf{M}^{(h)}|T^{(h)}, \sigma_\mu^2) \\ &\propto \exp\left((\mathbf{M}^{(h)} - \hat{\boldsymbol{\mu}}^{(h)})^T (\Omega^{(h)})^{-1} (\mathbf{M}^{(h)} - \hat{\boldsymbol{\mu}}^{(h)})\right), \end{aligned}$$

inducing that the conditional distribution of $\mathbf{M}^{(h)}$ is a multivariate Gaussian distribution with mean $\hat{\boldsymbol{\mu}}^{(h)}$ and covariance matrix $\Omega^{(h)}$:

$$\mathbf{M}^{(h)}|\mathbf{R}^{(h)}, T^{(h)}, \mathbf{A}^{(h)}, \sigma^2, \sigma_\mu^2 \sim \mathcal{N}\left(\hat{\boldsymbol{\mu}}^{(h)}, \Omega^{(h)}\right).$$

C The conditional distribution of σ^2

We have that

$$\begin{aligned} P(\sigma^2|\mathbf{T}, \mathbf{M}, Y, \mathbf{A}) &\propto P(Y|\mathbf{T}, \mathbf{M}, \sigma^2, \mathbf{A}) P(\sigma^2) \\ &\propto (\sigma^2)^{-1-\frac{n+v}{2}} \exp\left(-\frac{1}{\sigma^2} \left(\frac{1}{2} \sum_{i=1}^n \left(Y_i - \sum_{h=1}^m \sum_{l=1}^{L_h} \mu_{hl} \phi_{hl}(\mathbf{d}_i)\right)^2 + \frac{v\lambda}{2}\right)\right), \end{aligned}$$

inducing that the conditional distribution σ^2 is an Inverse-gamma distribution with shape $\frac{n+v}{2}$ and scale $\frac{1}{2} \sum_{i=1}^n \left(Y_i - \sum_{h=1}^m \sum_{l=1}^{L_h} \mu_{hl} \phi_{hl}(\mathbf{d}_i)\right)^2 + \frac{v\lambda}{2}$.

D The conditional distribution of σ_μ^2

We have that

$$\begin{aligned} P(\sigma_\mu^2|\mathbf{T}, \mathbf{M}, Y) &\propto P(\mathbf{M}|\mathbf{T}, \sigma_\mu^2) P(\sigma_\mu^2) \\ &\propto (\sigma_\mu^2)^{-\alpha_\mu - \frac{1}{2} \sum_{h=1}^m L_h} \exp\left(-\frac{1}{\sigma_\mu^2} \left(\frac{1}{2} \sum_{h=1}^m \sum_{l=1}^{L_h} \mu_{hl}^2 + \beta_\mu\right)\right), \end{aligned}$$

inducing that the conditional distribution of σ_μ^2 is an Inverse-gamma distribution with shape $\alpha_\mu + \frac{1}{2} \sum_{h=1}^m L_h$ and scale $\frac{1}{2} \sum_{h=1}^m \sum_{l=1}^{L_h} \mu_{hl}^2 + \beta_\mu$.

E The conditional distribution of \mathbf{p}_A given Sk-BAMDT

We have that

$$P(\mathbf{p}_A|\mathbf{T}, \mathbf{A}) \propto \prod_{h=1}^m \prod_{\eta} P(A_{\eta}^{(h)}|\mathbf{p}_A)P(\mathbf{p}_A) \propto \prod_{l=0}^k p_l^{\sum_h \sum_{\eta} \mathbb{1}(A_{\eta}^{(h)}=l) + \psi_l},$$

inducing that the conditional distribution of \mathbf{p}_A is a Dirichlet distribution :

$$\begin{aligned} P(\mathbf{p}_A|\mathbf{T}, \mathbf{A}) &\sim \text{Dirichlet}(\tilde{\boldsymbol{\psi}}) \\ \tilde{\boldsymbol{\psi}} &= (\tilde{\psi}_0, \dots, \tilde{\psi}_k) \\ \tilde{\psi}_l &= \sum_h \sum_{\eta} \mathbb{1}(A_{\eta}^{(h)} = l) + \psi_l. \end{aligned}$$

F The conditional distribution of p_A given S2-BAMDT

We have that

$$\begin{aligned} P(p_A|\mathbf{T}, \mathbf{A}) &\propto \prod_{h=1}^m \prod_{\eta} P(A_{\eta}^{(h)}|p_A)P(p_A) \\ &= p_A^{\sum_h \sum_{\eta} A_{\eta}^{(h)} + s_a - 1} (1 - p_A)^{\sum_h \sum_{\eta} (1 - A_{\eta}^{(h)}) + s_b - 1}, \end{aligned}$$

inducing that the conditional distribution of p_A is a Beta distribution :

$$p_A|\mathbf{T}, \mathbf{A} \sim \text{Beta}\left(\sum_h \sum_{\eta} A_{\eta}^{(h)} + s_a, \sum_h \sum_{\eta} (1 - A_{\eta}^{(h)}) + s_b\right).$$

G The conditional distribution of $A_{\eta}^{(h)}$ given Sk-BAMDT

We have that

$$\begin{aligned} P(A_{\eta}^{(h)}|T^{(h)}, \mathbf{p}_A, \mathbf{R}^{(h)}, \sigma^2, \sigma_{\mu}^2) &\propto P(\mathbf{R}^{(h)}|T^{(h)}, A_{\eta}^{(h)}, \sigma^2, \sigma_{\mu}^2)P(A_{\eta}^{(h)}|\mathbf{p}_A) \\ &= \prod_{l=0}^k (P(\mathbf{R}^{(h)}|T^{(h)}, A_{\eta}^{(h)} = l, \sigma^2, \sigma_{\mu}^2) p_l)^{\mathbb{1}(A_{\eta}^{(h)}=l)} \\ &\propto \prod_{l=0}^k \frac{p_l P(\mathbf{R}^{(h)}|T^{(h)}, A_{\eta}^{(h)} = l, \sigma^2, \sigma_{\mu}^2)}{\sum_j p_j P(\mathbf{R}^{(h)}|T^{(h)}, A_{\eta}^{(h)} = j, \sigma^2, \sigma_{\mu}^2)}, \end{aligned}$$

inducing that the conditional distribution of $A_{\eta}^{(h)}$ is a Multinomial distribution:

$$\begin{aligned} A_{\eta}^{(h)}|T^{(h)}, \mathbf{p}_A, \mathbf{R}^{(h)}, \sigma^2, \sigma_{\mu}^2 &\sim \text{Multinomial}(\mathbf{w}_{\mathbf{A}h}) \\ \mathbf{w}_{\mathbf{A}h} &= (w_{h0}, \dots, w_{hk}) \\ w_{hl} &= \frac{p_l P(\mathbf{R}^{(h)}|T^{(h)}, A_{\eta}^{(h)} = l, \sigma^2, \sigma_{\mu}^2)}{\sum_{j=0}^k p_j P(\mathbf{R}^{(h)}|T^{(h)}, A_{\eta}^{(h)} = j, \sigma^2, \sigma_{\mu}^2)}. \end{aligned}$$

H Proposals of Metropolis-Hastings for sampling the parameters $\{\alpha^{(h)}\}_{h=1}^m$

We describe the proposals of Metropolis-Hastings to sample $\alpha^{(h)}|T^{(h)}, \mathbf{M}^{(h)}, \mathbf{A}^{(h)}, \sigma^2, \sigma_\mu^2, \mathbf{R}^{(h)}$ (Algorithm 2). The chosen transition kernel q is a Gamma distribution with shape d and rate $d/\alpha^{(h)}$,

$$a_h^* \sim \text{Gamma}(d, d/\alpha^{(h)}),$$

where $\alpha^{(h)}$ is the value of the former iteration. In our simulation study, we have used $d = 20$. The Hastings ratio can be expressed as the product of three terms:

- *Transition ratio*

$$\text{TR} = \frac{q(\alpha^{(h)}|a_h^*)}{q(a_h^*|\alpha^{(h)})} = \frac{\left(\frac{1}{a_h^*}\right)^d (a^{(h)})^{d-1} \exp\left(-\frac{d}{a_h^*}\alpha^{(h)}\right)}{\left(\frac{1}{\alpha^{(h)}}\right)^d (a_h^*)^{d-1} \exp\left(-\frac{d}{\alpha^{(h)}}a_h^*\right)}$$

- *Prior ratio*

$$\text{PR} = \frac{P(a_h^*)}{P(\alpha^{(h)})} = \left(\frac{a_h^*}{\alpha^{(h)}}\right)^{\alpha_g-1} \exp(-\beta_g(a_h^* - \alpha^{(h)}))$$

- *Likelihood ratio*

$$\text{LR} = \frac{P(\mathbf{R}^{(h)}|\mathbf{M}^{(h)}, T^{(h)}, \mathbf{A}^{(h)}, a_h^*, \sigma^2)}{P(\mathbf{R}^{(h)}|\mathbf{M}^{(h)}, T^{(h)}, \mathbf{A}^{(h)}, \alpha^{(h)}, \sigma^2)}$$

Equation 4 is applied twice to generate LR: once for the ratio's denominator and once for its numerator.

Algorithm 2 Metropolis-Hastings Algorithm for sampling from the posterior $\alpha^{(h)}|T^{(h)}, \mathbf{M}^{(h)}, \mathbf{A}^{(h)}, \sigma^2, \sigma_\mu^2, \mathbf{R}^{(h)}$

Generate a candidate value a_h^* with probability $q(a_h^*|\alpha^{(h)})$.

Set $\alpha^{(h)} = a_h^*$ with probability

$$\min \left\{ 1, \frac{q(\alpha^{(h)}|a_h^*)}{q(a_h^*|\alpha^{(h)})} \frac{P(a_h^*)}{P(\alpha^{(h)})} \frac{P(\mathbf{R}^{(h)}|\mathbf{M}^{(h)}, T^{(h)}, \mathbf{A}^{(h)}, a_h^*, \sigma^2)}{P(\mathbf{R}^{(h)}|\mathbf{M}^{(h)}, T^{(h)}, \mathbf{A}^{(h)}, \alpha^{(h)}, \sigma^2)} \right\}$$

I Proposals of Metropolis-Hastings for sampling tree structures

We describe the proposals of Metropolis-Hastings to sample the tree structures.

I.0.0.1 GROW proposal This proposal randomly picks a terminal node, splits the chosen terminal node into two new nodes and assigns a decision rule to it. Let η be the randomly picked terminal node in tree $T^{(h)}$. The Hastings ratio can be expressed as the product of three terms:

- *Transition ratio*

$$\text{TR} = \frac{q(T^{(h)}|T^{(h)*})}{q(T^{(h)*}|T^{(h)})} = \frac{P(\text{PRUNE})N_s}{P(\text{GROW})N_m p_{rule}(\eta)},$$

where $p_{rule}(\eta)$ is the probability of a decision rule assigned to node η , N_m the number of internal nodes with two terminal children and N_s the number of terminal nodes in $T^{(h)}$.

- *Tree Structure ratio*

$$\text{TSR} = \frac{P(T^{(h)*})}{P(T^{(h)})} = \frac{\gamma(1+d_\eta)^{-\delta} (1-\gamma(2+d_\eta)^{-\delta})^2 p_{rule}(\eta)}{1-\gamma(1+d_\eta)^{-\delta}},$$

where d_η is the depth of node η .

- *Likelihood ratio*

$$\text{LR} = \frac{P(\mathbf{R}^{(h)}|T^{(h)*}, \sigma^2, \sigma_\mu^2, \mathbf{A}^{(h)*})}{P(\mathbf{R}^{(h)}|T^{(h)}, \sigma^2, \sigma_\mu^2, \mathbf{A}^{(h)})}$$

We apply Equation 5, considering the proposed tree, $T^{(h)*}$, and each of the potential interior node decisions, $A_\eta^{(h)}$. We also use Equation 5, considering the tree of the current iteration, $T^{(h)}$, and the determined interior node decisions of ancestors of η , $\mathbf{A}^{(h)}$.

$$\text{LR} = \begin{cases} \sum_{l=0}^k \frac{p_l P(\mathbf{R}^{(h)}|T^{(h)*}, \mathbf{A}^{(h)}, A_\eta^{(h)}=l, \sigma^2, \sigma_\mu^2)}{P(\mathbf{R}^{(h)}|T^{(h)}, \mathbf{A}^{(h)}, \sigma^2, \sigma_\mu^2)}, & \text{Sk-BAMDT} \\ \frac{p_A P(\mathbf{R}^{(h)}|T^{(h)*}, \mathbf{A}^{(h)}, A_\eta^{(h)}=1, \sigma^2, \sigma_\mu^2)}{P(\mathbf{R}^{(h)}|T^{(h)}, \mathbf{A}^{(h)}, \sigma^2, \sigma_\mu^2)} + \frac{(1-p_A) P(\mathbf{R}^{(h)}|T^{(h)*}, \mathbf{A}^{(h)}, A_\eta^{(h)}=0, \sigma^2, \sigma_\mu^2)}{P(\mathbf{R}^{(h)}|T^{(h)}, \mathbf{A}^{(h)}, \sigma^2, \sigma_\mu^2)}, & \text{S2-BAMDT} \end{cases}$$

I.0.0.2 PRUNE proposal This proposal randomly picks a parent of two terminal nodes and turns it into a terminal node by collapsing the nodes below it. Let η be the parent of two terminal nodes. The Hastings ratio can be expressed as the product of three terms:

- *Transition ratio*

$$\text{TR} = \frac{q(T^{(h)}|T^{(h)*})}{q(T^{(h)*}|T^{(h)})} = \frac{P(\text{GROW})N_m p_{rule}(\eta)}{P(\text{PRUNE})(N_s - 1)}$$

- *Tree structure ratio*

$$\text{TSR} = \frac{P(T^{(h)*})}{P(T^{(h)})} = \frac{1-\gamma(1+d_\eta)^{-\delta}}{\gamma(1+d_\eta)^{-\delta} (1-\gamma(2+d_\eta)^{-\delta})^2 p_{rule}(\eta)}$$

- *Likelihood ratio*

$$\text{LR} = \frac{P(\mathbf{R}^{(h)}|T^{(h)*}, \sigma^2, \sigma_\mu^2, \mathbf{A}^{(h)*})}{P(\mathbf{R}^{(h)}|T^{(h)}, \sigma^2, \sigma_\mu^2, \mathbf{A}^{(h)})}$$

Similar to the GROW proposal, LR is derived by applying Equation 5 twice, once for the numerator and once for the denominator of the ratio.

I.0.0.3 Change proposal This proposal randomly picks an internal node and randomly re-assigns to it a probabilistic decision. For simplicity we are restricted to picking an internal node having two terminal nodes as children. The Hastings ratio can be expressed as the product of three terms:

- *Transition ratio*

$$\text{TR} = \frac{q\left(A_\eta^{(h)} | A_\eta^{(h)*}\right)}{q\left(A_\eta^{(h)*} | A_\eta^{(h)}\right)} = 1$$

- *Assignment ratio*

$$\text{TAR} = \frac{P\left(A_\eta^{(h)*}\right)}{\left(A_\eta^{(h)}\right)} = \begin{cases} \frac{\prod_{j=0}^k p_j \mathbb{1}\left(A_\eta^{(h)*}=j\right)}{\prod_{l=0}^k p_l \mathbb{1}\left(A_\eta^{(h)}=l\right)}, & \text{Sk-BAMDT} \\ \frac{p_A^{A_\eta^{(h)*}} (1-p_A)^{1-A_\eta^{(h)*}}}{p_A^{A_\eta^{(h)}} (1-p_A)^{1-A_\eta^{(h)}}}, & \text{Method 2} \end{cases}$$

- *Likelihood ratio*

$$\text{LR} = \frac{P\left(\mathbf{R}^{(h)} | T^{(h)}, \sigma^2, \sigma_\mu^2, \mathbf{A}^{(h)(-\eta)}, A_\eta^{(h)*}\right)}{P\left(\mathbf{R}^{(h)} | T^{(h)}, \sigma^2, \sigma_\mu^2, \mathbf{A}^{(h)(-\eta)}, A_\eta^{(h)}\right)},$$

where $\mathbf{A}^{(h)(-\eta)} = \{A_b^{(h)}\}_{b \in T^{(h)}, b \neq \eta}$. Equation 5 is applied twice to generate LR: once for the ratio's denominator and once for its numerator.

J Inference Algorithm for S2-BAMDT

The primary difference between Sk-BAMDT and S2-BAMDT is how they handle probabilistic decisions for internal nodes. To infer the parameters $(\mathbf{T}, \mathbf{M}, \mathbf{A}, \boldsymbol{\alpha}, \sigma^2, \sigma_\mu^2, p_A)$, we suggest using a Metropolis-Hastings within block Gibbs sampler (Algorithm 3), similarly to Sk-BAMDT. The sampler requires m successive draws from $P\left(T^{(h)}, \mathbf{M}^{(h)}, \mathbf{A}^{(h)}, \boldsymbol{\alpha}^{(h)} | \sigma^2, \sigma_\mu^2, p_A, \mathbf{R}^{(h)}\right)$, followed by a draw of σ^2 from $P(\sigma^2 | \mathbf{T}, \mathbf{M}, \mathbf{A}, \mathbf{Y})$, a draw of σ_μ^2 from $P(\sigma_\mu^2 | \mathbf{T}, \mathbf{M}, \mathbf{A}, \mathbf{Y})$ and a draw of p_A from $P(p_A | \mathbf{T}, \mathbf{A})$. In Appendix H, we demonstrate the implementation of the Metropolis-Hastings algorithm that we propose to sample $\boldsymbol{\alpha}^{(h)} | T^{(h)}, \mathbf{M}^{(h)}, \mathbf{A}^{(h)}, \sigma^2, \sigma_\mu^2, \mathbf{R}^{(h)}$.

Then, we present the expressions for the posterior distributions of $A_\eta^{(h)}$ and p_A according to the assumptions of S2-BAMDT.

Theorem J.1. 1. *The conditional distribution of p_A is a Beta distribution:*

$$P(p_A | \mathbf{T}, \mathbf{A}) \sim \text{Beta}\left(\sum_h \sum_\eta A_\eta^{(h)} + s_a, \sum_h \sum_\eta (1 - A_\eta^{(h)}) + s_b\right).$$

2. The conditional distribution of $A_\eta^{(h)}$ is a Bernoulli distribution :

$$A_\eta^{(h)}|T^{(h)}, p_A, \mathbf{R}^{(h)}, \sigma^2, \sigma_\mu^2 \sim \text{Bernoulli}(w_{Ah})$$

$$w_{Ah} = \frac{p_A P\left(\mathbf{R}^{(h)}|T^{(h)}, A_\eta^{(h)} = 1, \sigma^2, \sigma_\mu^2\right)}{p_A P\left(\mathbf{R}^{(h)}|T^{(h)}, A_\eta^{(h)} = 1, \sigma^2, \sigma_\mu^2\right) + (1 - p_A) P\left(\mathbf{R}^{(h)}|T^{(h)}, A_\eta^{(h)} = 0, \sigma^2, \sigma_\mu^2\right)}.$$

Algorithm 3 Metropolis-Hastings within Gibbs sampler (S2-BAMDT)

```

for  $t = 1, 2, 3, \dots$  do
  for  $h = 1$  to  $m$  do
    Sample  $\alpha^{(h)}|T^{(h)}, \mathbf{M}^{(h)}, \mathbf{A}^{(h)}, \sigma^2, \sigma_\mu^2, \mathbf{R}^{(h)}$ 
    Sample  $T^{(h)}|\mathbf{R}^{(h)}, \sigma^2, \sigma_\mu^2, p_A$  using a Metropolis-Hastings Algorithm.
    If  $T^{(h)}$  grows, sample the probabilistic decision for the new internal node  $\eta$ ,
     $A_\eta^{(h)}|T^{(h)}, p_A, \mathbf{R}^{(h)}, \sigma^2, \sigma_\mu^2$ , from Bernoulli( $w_{Ah}$ ).
    Sample  $\mathbf{M}^{(h)}|\mathbf{R}^{(h)}, T^{(h)}, \mathbf{A}^{(h)}, \sigma^2, \sigma_\mu^2$  from  $\text{N}\left(\hat{\boldsymbol{\mu}}^{(h)}, \Omega^{(h)}\right)$ .
  end for
  Sample  $\sigma^2|\mathbf{T}, \mathbf{M}, \mathbf{A}, \mathbf{Y}$  from Inverse-Gamma( $s_{1\sigma}, s_{2\sigma}$ ).
  Sample  $\sigma_\mu^2|\mathbf{T}, \mathbf{M}, \mathbf{A}, \mathbf{Y}$  from Inverse-Gamma( $s_{1\mu}, s_{2\mu}$ ).
  Sample  $p_A|\mathbf{T}, \mathbf{A}$  from Beta  $\left(\sum_h \sum_\eta A_\eta^{(h)} + s_a, \sum_h \sum_\eta (1 - A_\eta^{(h)}) + s_b\right)$ .
end for

```

K U-shape Example 2

In that example, we also consider a 45 degree rotated U-shape domain using latitude and longitude as structured features. We generate ten unstructured features uniformly distributed in the interval $(0,1)$, $x_i \sim U(0,1)$. The U-shape domain is divided into three pieces by a circle with a radius of 0.9 centered at the origin. Assuming three Gaussian processes, we built a piecewise function $f(\cdot)$ that is dependent on (\mathbf{s}, x_1, x_2) and has separate covariance matrices derived by squared exponential covariance functions for each process. We assume a training data set of size $n = 800$ and a test data set of size $n_{test} = 300$. The responses in the training and test data are generated using Equation 1 at a noise level of $\sigma = 0.1$; 50 replicates are simulated. A random subset of 160 training data is used as knots for SBAMDT and BAMDT.

We discard the first 5000 iterations as burn-in and applied thinning by retaining one sample every five iterations from the remaining 5000 iterations of the MCMC algorithms in SBAMDT, BAMDT and BART. For SBART, we discard the first 8,000 iterations as burn-in and save 1000 samples after thinning.

The average performance measures of the benchmark models and SBAMDT over 50 replicates are summarised in Table 4, which shows that SBAMDT performs better than its competitors. The analysis highlights the need for making probabilistic decisions about hard or soft boundaries at each internal node as well as multivariate and soft splits in the feature space.

For a single randomly selected simulated test data set, the mean predictive surfaces, absolute percentage error (APE), CRPS and standard deviation (sd) of predictions from SBAMDT and

Table 4: The average performance metrics for SBAMDT and benchmark models over 50 replicates. Numbers in parenthesis correspond to the standard deviation of the forecasts among the different replicates associated with U-shape Example 2.

SBAMDT and Benchmark models					
	BAMDT	BART	SBART	Sk-BAMDT (q=6)	S2-BAMDT (q=4)
MAPE $\times 10^{-1}$	1.82(0.10)	2.06(0.10)	2.00(0.08)	1.49(0.10)	1.46 (0.10)
RMSPE $\times 10^{-1}$	2.50(0.16)	2.81(0.15)	2.72 (0.10)	2.13(0.15)	2.06 (0.17)
CRPS $\times 10^{-1}$	1.45(0.10)	1.65(0.09)	1.53(0.06)	1.13 (0.07)	1.14(0.08)

benchmark models are shown in Figures 10, 11, 12 and 13. The results show that SBAMDT produces predictions with less uncertainty and offers the best fit to the ground truth. Within clusters, SBAMDT operates very well with low errors close to the cluster boundary. We don't see that behaviour in its competitors, which supports SBAMDT's win. Using one of the fifty simulated data sets, Figure 14 displays the significance metric for both structured and unstructured characteristics for every model. Similar to our other simulation results, SBAMDT prioritize the non-noisy features.

L Proof of Theorem 1

1. We consider that \mathbf{T} and \mathbf{A} are known. For μ_{hl} , we have used a normal prior with a zero mean and variance σ_μ^2 . The variance σ_μ^2 is subjected to an inverse-Gamma prior with hyper-parameters α_μ and β_μ .

The expected value of f by integrating the function over the prior distribution of \mathbf{M} is given by:

$$E(f(\mathbf{d})|\mathbf{T}, \mathbf{A}) = \sum_{h=1}^m \sum_{l=1}^{L_h} \phi_{hl}(\mathbf{d}) E(\mu_{hl}|T^{(h)}) = 0. \quad (6)$$

The covariance function of f with respect to the prior distribution of \mathbf{M} is given by:

$$\begin{aligned} C(f_i, f_j) &= E((f(\mathbf{d}_i) - 0)(f(\mathbf{d}_j) - 0)|\mathbf{T}, \mathbf{A}) \\ &= \sum_{h=1}^m \sum_{l=1}^{L_h} \phi_{hl}(\mathbf{d}_i) \phi_{hl}(\mathbf{d}_j) \text{Var}(\mu_{hl}) \\ &= \frac{\beta_\mu}{\alpha_\mu - 1} \sum_{h=1}^m \sum_{l=1}^{L_h} \phi_{hl}(\mathbf{d}_i) \phi_{hl}(\mathbf{d}_j). \end{aligned}$$

The gradient of f with respect to \mathbf{d} is given as follows:

$$\nabla_{\mathbf{d}} f(\mathbf{d}) = \sum_{h=1}^m \sum_{l=1}^{L_h} \mu_{hl} \nabla_{\mathbf{d}} \phi_{hl}(\mathbf{d}).$$

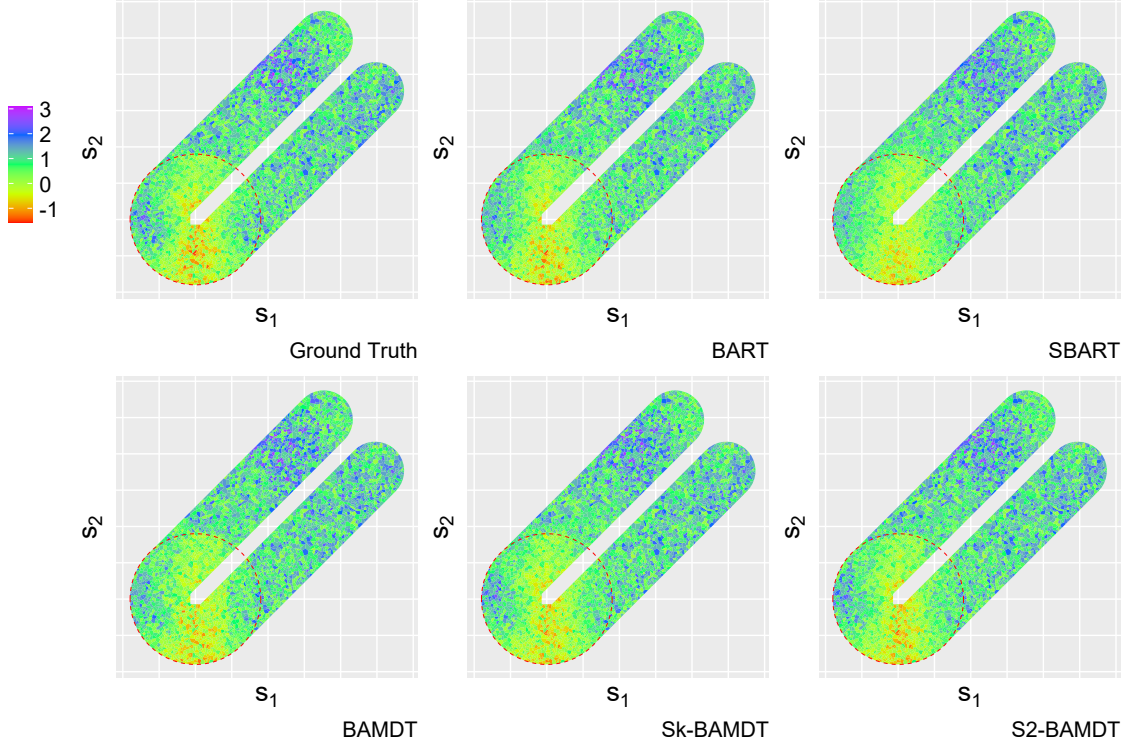


Figure 10: The ground truth for $f(\mathbf{s}, \mathbf{x})$ and the spatial of SBAMDT, BAMDT, BART and SBART associated with U-shape Example 2. Red dashed circle indicate discontinuity surfaces in the true function projected to \mathcal{M} .

We use the product rule to find the gradient of the probability of a data point \mathbf{d} falling into the terminal node l :

$$\begin{aligned} \nabla_{\mathbf{d}} \phi_{hl}(\mathbf{d}) &= \sum_{\eta \in P_{hl}(\mathbf{d})} \nabla_{\mathbf{d}} P_{\eta}(\mathbf{d}; A_{\eta}^{(h)}) \prod_{v \in P_{hl}(\mathbf{d}), v \neq \eta} P_v(\mathbf{d}; A_v^{(h)}), \quad \text{where} \\ \nabla_{\mathbf{d}} P_{\eta}(\mathbf{d}; A_{\eta}^{(h)}) &= \left(\nabla_{\mathbf{d}} [z_{\eta L}^{(h)}(\mathbf{d}) | A_{\eta}^{(h)}] \right)^{\mathbb{1}(r_{\eta L}^{(h)}=1)} \left(- \nabla_{\mathbf{d}} [z_{\eta L}^{(h)}(\mathbf{d}) | A_{\eta}^{(h)}] \right)^{1-\mathbb{1}(r_{\eta L}^{(h)}=1)}. \end{aligned}$$

- (a) **Univariate split:** Let x_i be the uniformly chosen unstructured feature, and x_{iL}^* and x_{iR}^* the values of the i th unstructured feature for the nearest left and right knot at node η . For a univariate split, the derivative of the decision rule function $[z_{\eta L}^{(h)}(\mathbf{d}) | A_{\eta}^{(h)}]$ is given by:

$$\nabla_{\mathbf{d}} [z_{\eta L}^{(h)}(\mathbf{d}) | A_{\eta}^{(h)}] \neq 0 = \begin{bmatrix} 0 \\ \vdots \\ C_i \\ \vdots \\ 0 \end{bmatrix}.$$

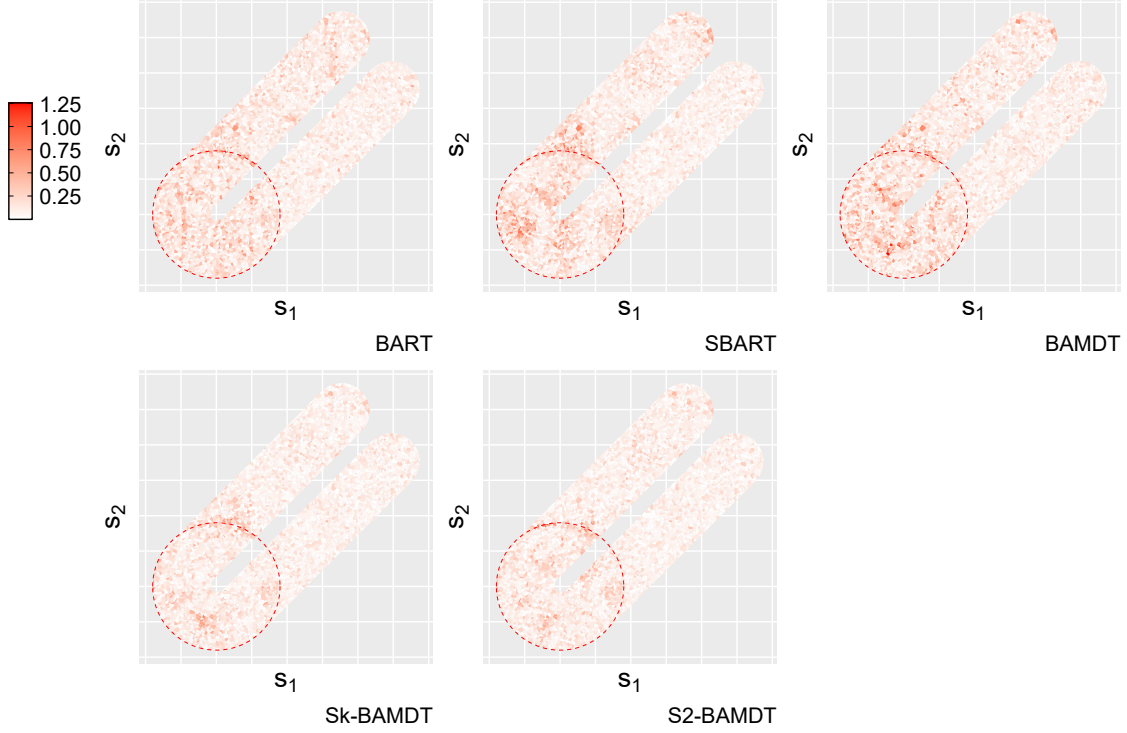


Figure 11: The APE of SBAMDT, BAMDT, BART and SBART associated with U-shape Example 2.

i. Soft split ($A_\eta^{(h)} \neq 0$):

$$\begin{aligned}
C_i &= \frac{d \left(1 + e^{-\alpha_c^{(h)} \frac{|x_i - x_{iR}^*| - |x_i - x_{iL}^*|}{C_\eta^{(h)}}} \right)^{-1}}{dx_i} \\
&= \left(1 + e^{-\alpha_c^{(h)} \frac{|x_i - x_{iR}^*| - |x_i - x_{iL}^*|}{C_\eta^{(h)}}} \right)^{-2} e^{-\alpha_c^{(h)} \frac{|x_i - x_{iR}^*| - |x_i - x_{iL}^*|}{C_\eta^{(h)}}} \\
&\quad \times \frac{2\alpha_c^{(h)}}{C_\eta^{(h)}} \left(-\mathbb{1}(x_{iL}^* < x_i < x_{iR}^*) + \mathbb{1}(x_{iR}^* < x_i < x_{iL}^*) \right). \tag{7}
\end{aligned}$$

ii. Hard split ($A_\eta^{(h)} = 0$):

$$C_i = -\delta \left(x_i - \frac{x_{iR}^* + x_{iL}^*}{2} \right) \mathbb{1}(x_{iL}^* < x_i < x_{iR}^*) + \delta \left(x_i - \frac{x_{iR}^* + x_{iL}^*}{2} \right) \mathbb{1}(x_{iR}^* < x_i < x_{iL}^*),$$

where $\delta(\cdot)$ denotes the Dirac delta function. The partial derivative with respect to x_i is 0 except for $x_i = \frac{x_{iR}^* + x_{iL}^*}{2}$, where the impulse makes the derivative undefined. SBAMDT can, however, approach the hard split via a soft split if the softness control parameter $\alpha_c^{(h)}$ is set to infinity.

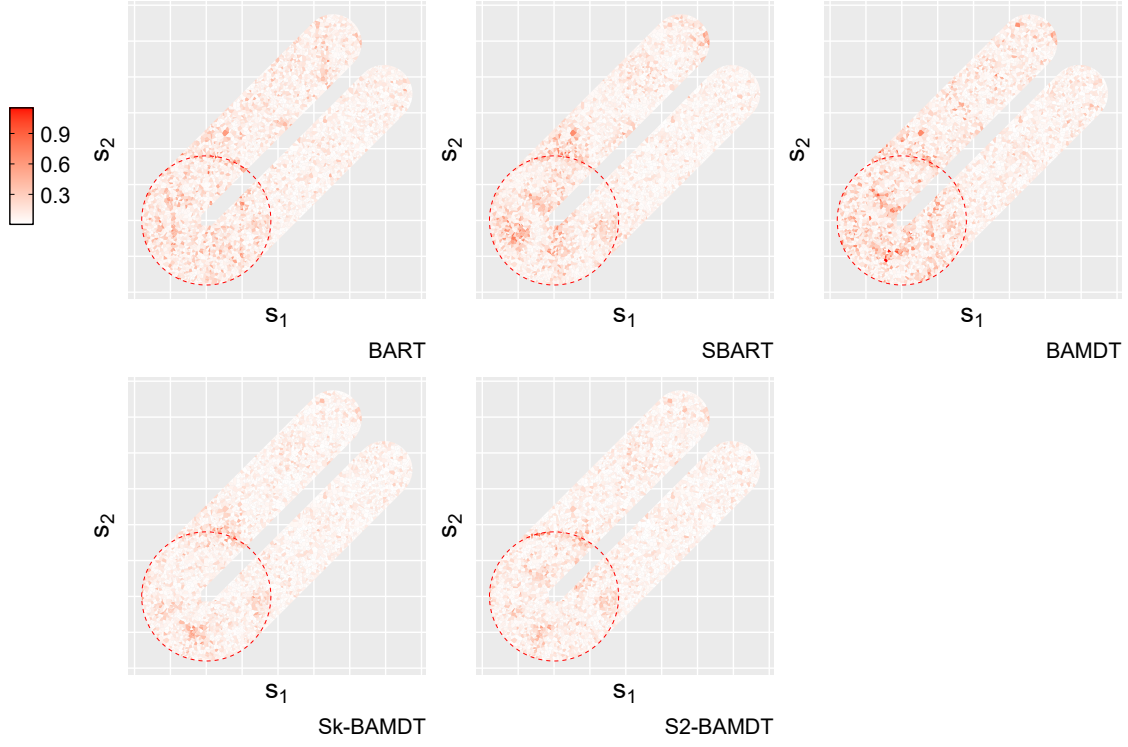


Figure 12: The CRPS of SBAMDT, BAMDT, BART and SBART associated with U-shape Example 2.

(b) **Multivariate split:** Let \mathbf{s}_L^* and \mathbf{s}_R^* be the structured feature of the nearest left and right knot at node η . For multivariate splits:

i. Soft split ($A_\eta^{(h)} \neq 0$):

$$\begin{aligned}
C_s &= \nabla \mathbf{s} \left(1 + e^{-\frac{\alpha_c^{(h)} \|\mathbf{s} - \mathbf{s}_R^*\|_2 - \|\mathbf{s} - \mathbf{s}_L^*\|_2}{C_\eta^{(h)}}} \right)^{-1} \\
&= \left(1 + e^{-\frac{\alpha_c^{(h)} \|\mathbf{s} - \mathbf{s}_R^*\|_2 - \|\mathbf{s} - \mathbf{s}_L^*\|_2}{C_\eta^{(h)}}} \right)^{-2} e^{-\frac{\alpha_c^{(h)} \|\mathbf{s} - \mathbf{s}_R^*\|_2 - \|\mathbf{s} - \mathbf{s}_L^*\|_2}{C_\eta^{(h)}}} \\
&\quad \times \left(\frac{\alpha_c^{(h)}}{C_\eta^{(h)}} \right) \left(\frac{\mathbf{s} - \mathbf{s}_R^*}{\|\mathbf{s} - \mathbf{s}_R^*\|_2} - \frac{\mathbf{s} - \mathbf{s}_L^*}{\|\mathbf{s} - \mathbf{s}_L^*\|_2} \right). \tag{8}
\end{aligned}$$

ii. Hard split ($A_\eta^{(h)} = 0$):

$$C_s = -\delta \left((\mathbf{s}_R^* - \mathbf{s}_L^*)^T \mathbf{s} - \frac{\mathbf{s}_R^{*T} \mathbf{s}_R^* - \mathbf{s}_L^{*T} \mathbf{s}_L^*}{2} \right) (\mathbf{s}_R^* - \mathbf{s}_L^*). \tag{9}$$

The derivative does not exist at:

$$(\mathbf{s}_R^* - \mathbf{s}_L^*)^T \mathbf{s} = \frac{\mathbf{s}_R^{*T} \mathbf{s}_R^* - \mathbf{s}_L^{*T} \mathbf{s}_L^*}{2}.$$

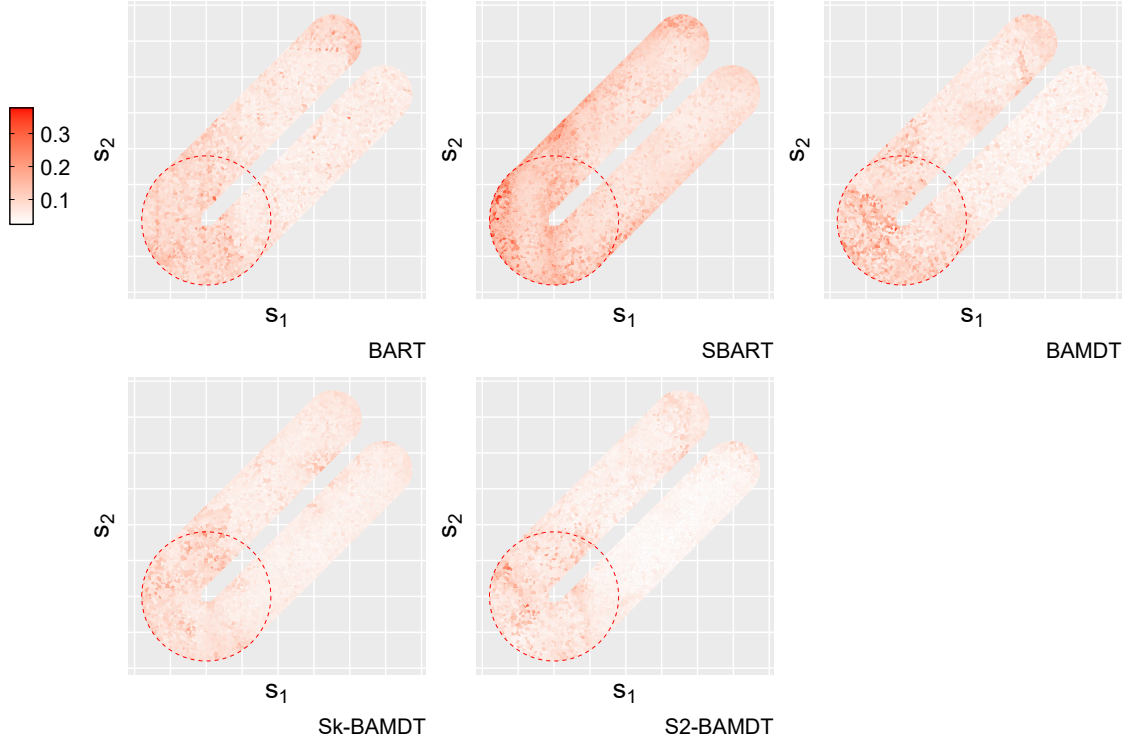


Figure 13: The sd of SBAMDT, BAMDT, BART and SBART associated with U-shape Example 2.

2. We assume that \mathbf{T} is known. The expected value of $g^{(h)}(\mathbf{d}) = \sum_{l=1}^{L_h} \mu_{hl} \phi_{hl}(\mathbf{d})$, when integrated over the prior distributions of \mathbf{M} and \mathbf{A} , is given by:

$$E(g^{(h)}(\mathbf{d})) = \sum_{l=1}^{L_h} E(\mu_{hl} \phi_{hl}(\mathbf{d}) | \mathbf{T}^{(h)}) = 0.$$

The variance of $g^{(h)}(\mathbf{d})$ is:

$$\text{Var}(g^{(h)}(\mathbf{d})) = \sum_{l=1}^{L_h} \text{Var}(\mu_{hl}) E(\phi_{hl}^2(\mathbf{d})) < \infty.$$

By the Central Limit Theorem (CLT), as the number of trees m goes to infinity, the function $f(\mathbf{d}) = \sum_{h=1}^m g^{(h)}(\mathbf{d})$ approaches a normal distribution with:

- **Mean:** $\sum_{h=1}^m E(g^{(h)}(\mathbf{d}))$,
- **Variance:** $\sum_{h=1}^m \text{Var}(g^{(h)}(\mathbf{d}))$.

Thus, as $m \rightarrow \infty$, we can model the prior of f as a ****Gaussian Process (GP)****, where the expected value of $f(\mathbf{d})$, integrating over the prior distributions of \mathbf{M} and \mathbf{A} , is:

$$E(f(\mathbf{d}) | \mathbf{T}) = \sum_{h=1}^m \sum_{l=1}^{L_h} E(\mu_{hl} \phi_{hl}(\mathbf{d}) | \mathbf{T}^{(h)}) = \sum_{h=1}^m \sum_{l=1}^{L_h} E(\mu_{hl} | \mathbf{T}^{(h)}) E(\phi_{hl}(\mathbf{d})) = 0.$$

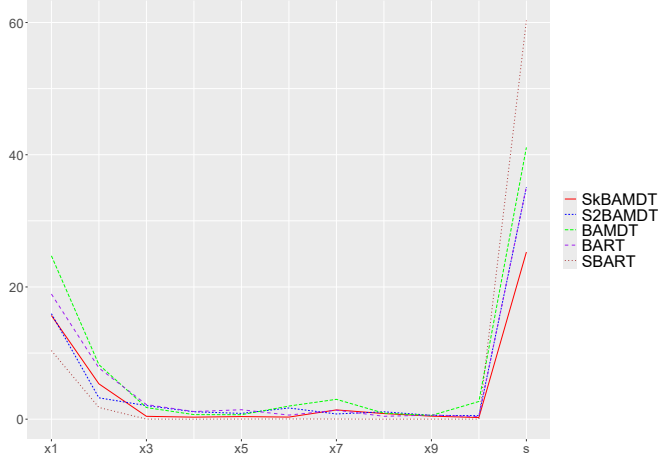


Figure 14: The importance metric for each feature given by Sk-BAMDT, S2-BAMDT, BAMDT, BART and SBART associated with U-shape Example 2.

The covariance function between $f(\mathbf{d}_i)$ and $f(\mathbf{d}_j)$ with respect to the prior distributions of \mathbf{M} and \mathbf{A} is:

$$C(f(\mathbf{d}_i), f(\mathbf{d}_j)) = E[(f(\mathbf{d}_i) - 0)(f(\mathbf{d}_j) - 0) | \mathbf{T}] = \sum_{h=1}^m \sum_{l=1}^{L_h} E(\phi_{hl}(\mathbf{d}_i)\phi_{hl}(\mathbf{d}_j)) \text{Var}(\mu_{hl}).$$

Since μ_{hl} follows a prior distribution with variance $\text{Var}(\mu_{hl}) = \frac{\beta_\mu}{\alpha_\mu - 1}$, we can express the covariance as:

$$C(f(\mathbf{d}_i), f(\mathbf{d}_j)) = \frac{\beta_\mu}{\alpha_\mu - 1} \sum_{h=1}^m \sum_{l=1}^{L_h} E(\phi_{hl}(\mathbf{d}_i)\phi_{hl}(\mathbf{d}_j)).$$

Next, we compute $E(\phi_{hl}(\mathbf{d}_i)\phi_{hl}(\mathbf{d}_j))$. This expectation can be written as:

$$E(\phi_{hl}(\mathbf{d}_i)\phi_{hl}(\mathbf{d}_j)) = E(\phi_{hl}(\mathbf{d}_i; \mathbf{A}^{(h)})\phi_{hl}(\mathbf{d}_j; \mathbf{A}^{(h)})).$$

Expanding this expectation as a product over all indices $\eta \in P_{hl}(\mathbf{d}_i)$, we get:

$$E(\phi_{hl}(\mathbf{d}_i)\phi_{hl}(\mathbf{d}_j)) = \prod_{\eta \in P_{hl}(\mathbf{d}_i)} \int dA_\eta^{(h)} P(A_\eta^{(h)}) P_\eta(\mathbf{d}_i; A_\eta^{(h)}) P_\eta(\mathbf{d}_j; A_\eta^{(h)}).$$

This simplifies to:

$$E(\phi_{hl}(\mathbf{d}_i)\phi_{hl}(\mathbf{d}_j)) = \prod_{\eta \in P_{hl}(\mathbf{d}_i)} \sum_{v=0}^k P_\eta(\mathbf{d}_i; A_\eta^{(h)} = v) P_\eta(\mathbf{d}_j; A_\eta^{(h)} = v) P(A_\eta^{(h)} = v).$$

Thus, the covariance between $f(\mathbf{d}_i)$ and $f(\mathbf{d}_j)$ can be compactly expressed as:

$$C(f(\mathbf{d}_i), f(\mathbf{d}_j)) = \frac{\beta_\mu}{\alpha_\mu - 1} \sum_{h=1}^m \sum_{l=1}^{L_h} \prod_{\eta \in P_{hl}(\mathbf{d}_i)} \sum_{v=0}^k P_\eta(\mathbf{d}_i; A_\eta^{(h)} = v) P_\eta(\mathbf{d}_j; A_\eta^{(h)} = v) P(A_\eta^{(h)} = v).$$

3. Conditional on $\{\hat{\mathbf{T}}, \hat{\mathbf{M}}^{(-h)}, \hat{\mathbf{A}}, \hat{\sigma}^2, \hat{\sigma}_\mu^2\}$, we have that:

$$f(\mathbf{d}) = \mathbf{M}^{(h)T} \hat{\Phi}^{(h)}(\mathbf{d}) + \sum_{h'=1, h' \neq h}^m \hat{\mathbf{M}}^{(h')T} \hat{\Phi}^{(h')}(\mathbf{d}).$$

The conditional distribution of $\mathbf{M}^{(h)}$ is a multivariate Gaussian distribution with a mean $\hat{\boldsymbol{\mu}}^{(h)}$ and covariance matrix $\Omega^{(h)}$. The expected value of $f(\mathbf{d})$, by integrating the function over the conditional distribution of $\mathbf{M}^{(h)}$, is given by:

$$\begin{aligned} \hat{\mu}_f^{(h)}(\mathbf{d}) &= E\left(f(\mathbf{d}) \mid \hat{T}, \hat{\mathbf{M}}^{(-h)}, \hat{\mathbf{A}}, \hat{\sigma}^2, \hat{\sigma}_\mu^2, \mathbf{Y}\right) \\ &= \hat{\boldsymbol{\mu}}^{(h)T} \hat{\Phi}^{(h)}(\mathbf{d}) + \sum_{h'=1, h' \neq h}^m \hat{\mathbf{M}}^{(h')T} \hat{\Phi}^{(h')}(\mathbf{d}). \end{aligned}$$

This implies that:

$$f(\mathbf{d}) - \hat{\mu}_f^{(h)}(\mathbf{d}) = (\mathbf{M}^{(h)} - \hat{\boldsymbol{\mu}}^{(h)})^T \hat{\Phi}^{(h)}(\mathbf{d}),$$

The covariance function of f with respect to the conditional distribution of $\mathbf{M}^{(h)}$ is:

$$\begin{aligned} \hat{C}(f_i, f_j) &= E\left(\left(f(\mathbf{d}_i) - \hat{\mu}_f^{(h)}(\mathbf{d}_i)\right) \left(f(\mathbf{d}_j) - \hat{\mu}_f^{(h)}(\mathbf{d}_j)\right) \mid \hat{T}, \hat{\mathbf{M}}^{(-h)}, \hat{\mathbf{A}}, \hat{\sigma}^2, \hat{\sigma}_\mu^2, \mathbf{Y}\right) \\ &= \hat{\Phi}^{(h)T}(\mathbf{d}_i) E\left(\left(\mathbf{M}^{(h)} - \hat{\boldsymbol{\mu}}^{(h)}\right) \left(\mathbf{M}^{(h)} - \hat{\boldsymbol{\mu}}^{(h)}\right)^T \mid \hat{T}, \hat{\mathbf{M}}^{(-h)}, \hat{\mathbf{A}}, \hat{\sigma}^2, \hat{\sigma}_\mu^2, \mathbf{Y}\right) \hat{\Phi}^{(h)}(\mathbf{d}_j) \\ &= \hat{\Phi}^{(h)T}(\mathbf{d}_i) \Omega^{(h)} \hat{\Phi}^{(h)}(\mathbf{d}_j). \end{aligned}$$

M NYC Education

This appendix contains figures that showcase the importance metrics for both structured and unstructured features for each model assessed. We also include the marginal influence of individuals over 25 with higher educational attainment, represented on the original scale.

N Simulation study on synthetic data

This appendix displays a figure that presents the significance metrics for both structured and unstructured features across all models, utilizing one of the fifty simulated datasets for the U-shape example.

References

Hugh A Chipman, Edward I George, and Robert E McCulloch. Bart: Bayesian additive regression trees. 2010.

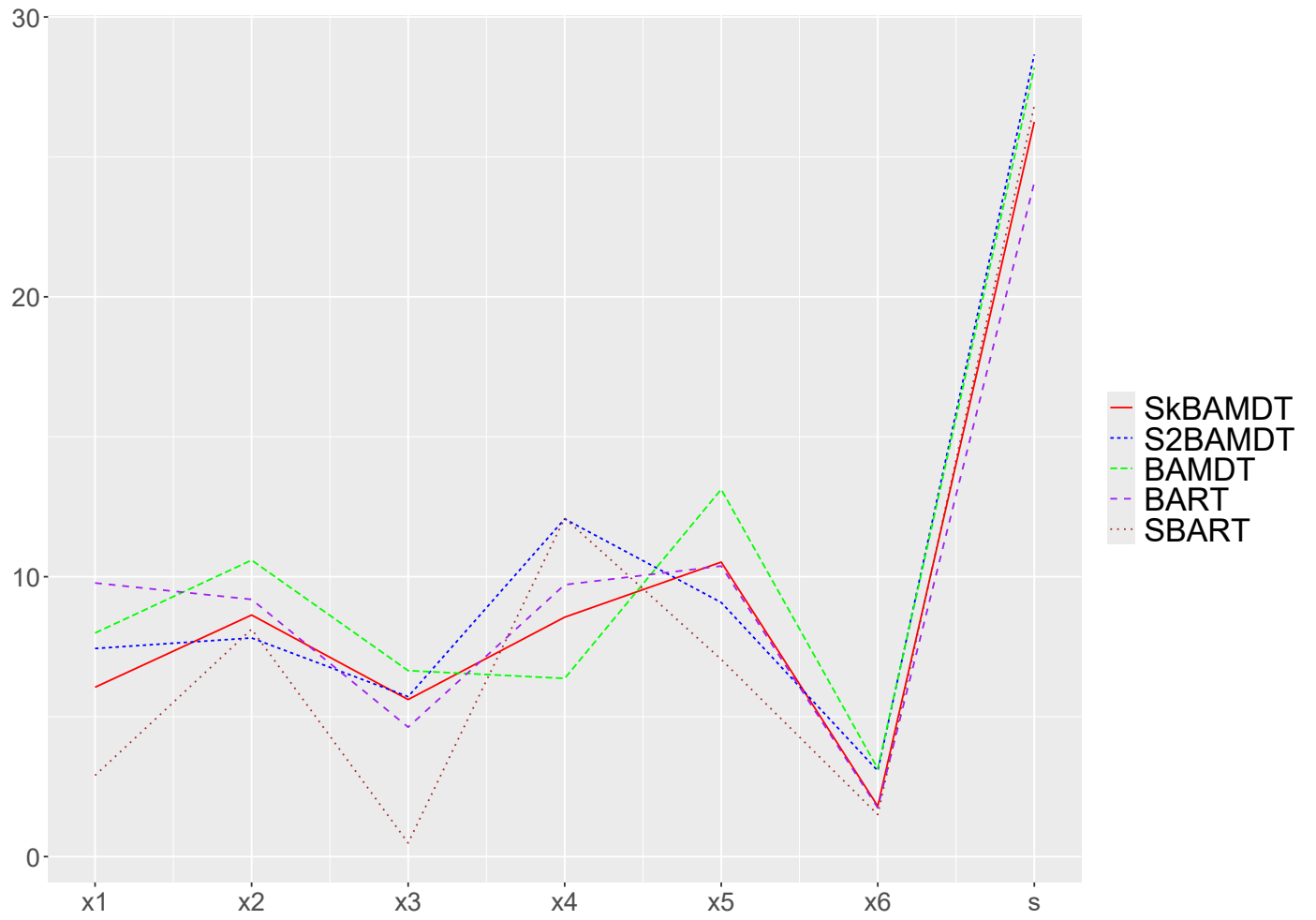


Figure 15: The importance metric for each feature given by Sk-BAMDT, S2-BAMDT, BAMDT, BART and SBART.

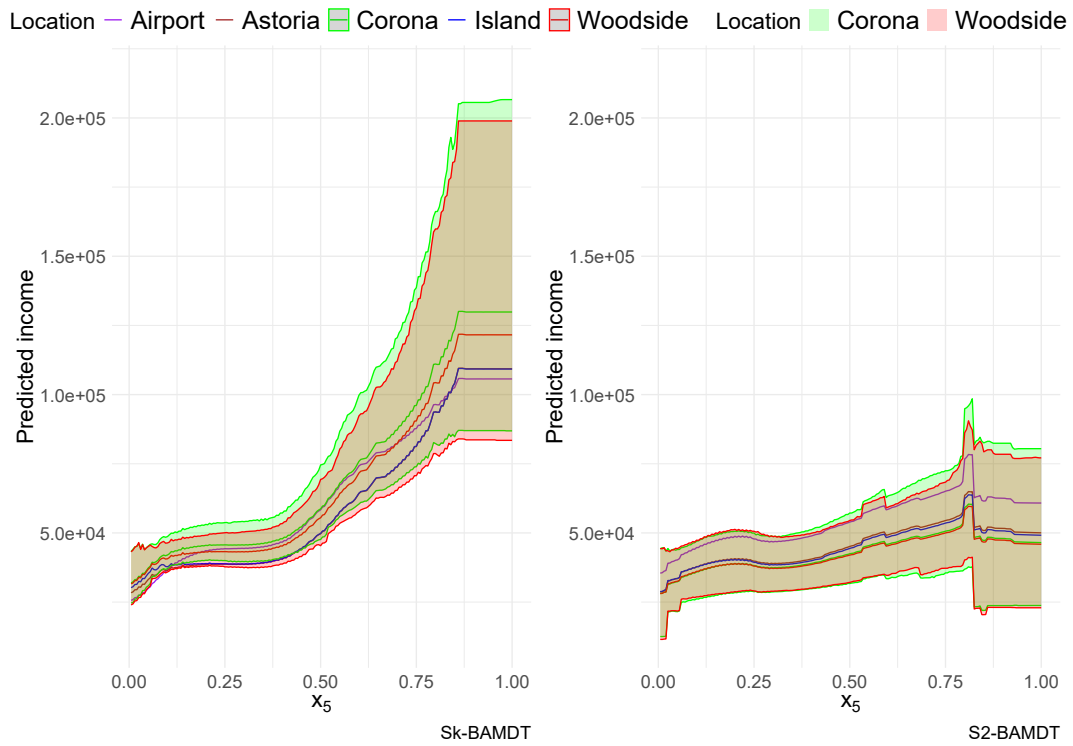


Figure 16: The predicted income versus the population over 25 with at least a bachelor’s degree. Colored ribbons represent 95% predictive credible intervals of two representative locations.

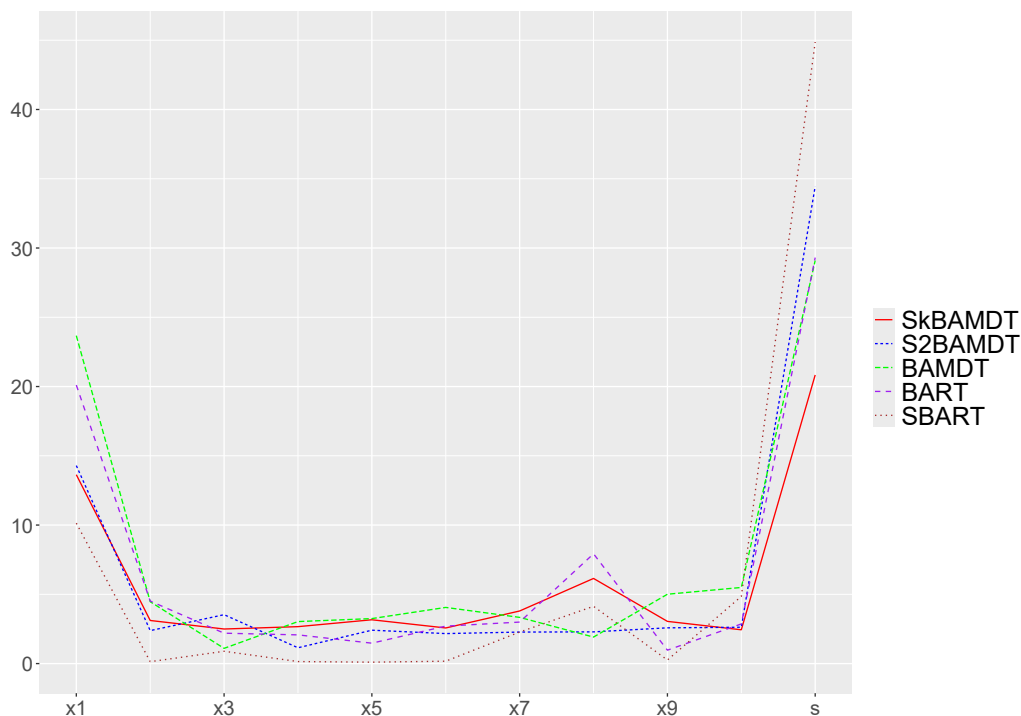


Figure 17: The importance metric for each feature for one U-shape simulation.

Yoav Freund and Robert E Schapire. A decision-theoretic generalization of on-line learning and an application to boosting. *Journal of computer and system sciences*, 55(1):119–139, 1997.

Leo Breiman. Bagging predictors. *Machine learning*, 24:123–140, 1996.

Leo Breiman. Random forests. *Machine learning*, 45:5–32, 2001.

Junni L Zhang and Wolfgang K Härdle. The Bayesian additive classification tree applied to credit risk modelling. *Computational Statistics & Data Analysis*, 54(5):1197–1205, 2010.

Bereket P Kindo, Hao Wang, and Edsel A Peña. Multinomial probit Bayesian additive regression trees. *Stat*, 5(1):119–131, 2016.

Justin Bleich, Adam Kapelner, Edward I George, Shane T Jensen, et al. Variable selection for BART: an application to gene regulation. *The Annals of Applied Statistics*, 8(3):1750–1781, 2014.

Antonio R Linero. Bayesian regression trees for high-dimensional prediction and variable selection. *Journal of the American Statistical Association*, 113(522):626–636, 2018.

Hugh A Chipman, Edward I George, Robert E McCulloch, and Thomas S Shively. mBART: Multidimensional Monotone BART. *Bayesian Analysis*, 1(1):1–30, 2021.

Jennifer L Hill. Bayesian nonparametric modeling for causal inference. *Journal of Computational and Graphical Statistics*, 20(1):217–240, 2011.

- Rodney A Sparapani, Brent R Logan, Robert E McCulloch, and Purushottam W Laud. Nonparametric survival analysis using Bayesian additive regression trees (BART). *Statistics in Medicine*, 35(16):2741–2753, 2016.
- Justin Bleich and Adam Kapelner. Bayesian Additive Regression Trees with Parametric Models of Heteroskedasticity. *arXiv preprint arXiv:1402.5397*, 2014.
- Matthew T Pratola et al. Efficient Metropolis–Hastings proposal mechanisms for Bayesian regression tree models. *Bayesian Analysis*, 11(3):885–911, 2016.
- Jared S Murray. Log-linear Bayesian additive regression trees for multinomial logistic and count regression models. *Journal of the American Statistical Association*, 116(534):756–769, 2021.
- Stamatina Lamprinakou, Mauricio Barahona, Seth Flaxman, Sarah Filippi, Axel Gandy, and Emma J McCoy. Bart-based inference for poisson processes. *Computational Statistics & Data Analysis*, 180:107658, 2023.
- Veronika Ročková and Stéphanie van der Pas. Posterior concentration for Bayesian regression trees and forests. *The Annals of Statistics*, 48(4):2108 – 2131, 2020.
- Veronika Ročková and Enakshi Saha. On Theory for BART. In Kamalika Chaudhuri and Masashi Sugiyama, editors, *Proceedings of the Twenty-Second International Conference on Artificial Intelligence and Statistics*, volume 89 of *Proceedings of Machine Learning Research*, pages 2839–2848. PMLR, 16–18 Apr 2019. URL <https://proceedings.mlr.press/v89/rockova19a.html>.
- Antonio R Linero and Yun Yang. Bayesian regression tree ensembles that adapt to smoothness and sparsity. *Journal of the Royal Statistical Society: Series B (Statistical Methodology)*, 80(5): 1087–1110, 2018.
- Shufei Ge, Shijia Wang, Yee Whye Teh, Liangliang Wang, and Lloyd Elliott. Random tessellation forests. In H. Wallach, H. Larochelle, A. Beygelzimer, F. d'Alché-Buc, E. Fox, and R. Garnett, editors, *Advances in Neural Information Processing Systems*, volume 32. Curran Associates, Inc., 2019.
- Xuhui Fan, Bin Li, Yi Wang, Yang Wang, and Fang Chen. The Ostomachion Process. In *Proceedings of the AAAI Conference on Artificial Intelligence*, volume 30, 2016.
- Tyler M Tomita, James Browne, Cencheng Shen, Jaewon Chung, Jesse L Patsolic, Benjamin Falk, Carey E Priebe, Jason Yim, Randal Burns, Mauro Maggioni, et al. Sparse projection oblique randomer forests. *Journal of Machine Learning Research*, 21(104), 2020.
- Tom Rainforth and Frank Wood. Canonical correlation forests. *arXiv preprint arXiv:1507.05444*, 2015.
- Juan José Rodríguez, Ludmila I Kuncheva, and Carlos J Alonso. Rotation forest: A new classifier ensemble method. *IEEE Transactions on Pattern Analysis and Machine Intelligence*, 28(10): 1619–1630, 2006.
- Rico Blaser and Piotr Fryzlewicz. Regularizing axis-aligned ensembles via data rotations that favor simpler learners. *Statistics and Computing*, 2021.

- Rico Blaser and Piotr Fryzlewicz. Random rotation ensembles. *The Journal of Machine Learning Research*, 2016.
- Adam J Stone and John Paul Gosling. Addivortes:(bayesian) additive voronoi tessellations. *Journal of Computational and Graphical Statistics*, (just-accepted):1–19, 2024.
- Mateus Maia, Keefe Murphy, and Andrew C. Parnell. Gp-bart: A novel bayesian additive regression trees approach using gaussian processes. *Computational Statistics & Data Analysis*, 190:107858, 2024. ISSN 0167-9473. doi: <https://doi.org/10.1016/j.csda.2023.107858>. URL <https://www.sciencedirect.com/science/article/pii/S016794732300169X>.
- Zhao Tang Luo, Huiyan Sang, and Bani Mallick. Bamdt: Bayesian additive semi-multivariate decision trees for nonparametric regression. In *International Conference on Machine Learning*, pages 14509–14526. PMLR, 2022.
- Keenan Crane, Marco Livesu, Enrico Puppo, and Yipeng Qin. A survey of algorithms for geodesic paths and distances. *arXiv preprint arXiv:2007.10430*, 2020.
- Jianbo Shi and Jitendra Malik. Normalized cuts and image segmentation. *IEEE Transactions on pattern analysis and machine intelligence*, 22(8):888–905, 2000.
- Ronald R Coifman and Stéphane Lafon. Diffusion maps. *Applied and computational harmonic analysis*, 21(1):5–30, 2006.
- Mikhail Belkin and Partha Niyogi. Laplacian eigenmaps for dimensionality reduction and data representation. *Neural computation*, 15(6):1373–1396, 2003.
- F Göbel and AA Jagers. Random walks on graphs. *Stochastic processes and their applications*, 2(4):311–336, 1974.
- David B Dunson, Hau-Tieng Wu, and Nan Wu. Graph based gaussian processes on restricted domains. *Journal of the Royal Statistical Society Series B: Statistical Methodology*, 84(2):414–439, 2022.
- Andrew Gelman, Jessica Hwang, and Aki Vehtari. Understanding predictive information criteria for bayesian models. *Statistics and computing*, 24:997–1016, 2014.
- Jingyu He and P Richard Hahn. Stochastic tree ensembles for regularized nonlinear regression. *Journal of the American Statistical Association*, 118(541):551–570, 2023.
- Theodore Edward Harris et al. *The theory of branching processes*, volume 6. Springer Berlin, 1963.
- Meijia Wang, Jingyu He, and P Richard Hahn. Local gaussian process extrapolation for bart models with applications to causal inference. *Journal of Computational and Graphical Statistics*, 33(2): 724–735, 2024.
- Trevor Hastie and Robert Tibshirani. Bayesian backfitting (with comments and a rejoinder by the authors). *Statistical Science*, 15(3):196–223, 2000.

Tilmann Gneiting and Adrian E Raftery. Strictly proper scoring rules, prediction, and estimation.
Journal of the American statistical Association, 102(477):359–378, 2007.

GeoDa Data and Lab. URL :https://geodacenter.github.io/data-and-lab/NYC_Tract_ACS_2008_12/.